ACS ES&T Air

Open Access

pubs.acs.org/estair

Article

Rapid Nucleation and Growth of Indoor Atmospheric Nanocluster Aerosol during the Use of Scented Volatile Chemical Products in Residential Buildings

Satya S. Patra, Jianghui Liu, Jinglin Jiang, Xiaosu Ding, Chunxu Huang, Connor Keech, Gerhard Steiner, Philip S. Stevens, Nusrat Jung, and Brandon E. Boor*

Cite This: *ACS EST Air* 2024, 1, 1276−1293

Read Online

ACCESS | Metrics & More | Article Recommendations | Supporting Information

ABSTRACT: Scented volatile chemical products (sVCPs) are frequently used indoors. We conducted field measurements in a residential building to investigate new particle formation (NPF) from sVCP emissions. State-of-the-art instrumentation was used for real-time monitoring of indoor atmospheric nanocluster aerosol (NCA; 1−3 nm particles) size distributions and terpene mixing ratios. We integrated our NCA measurements with a comprehensive material balance model to analyze sVCP-nucleated indoor NCA dynamics. Our results reveal that sVCPs significantly increase indoor terpene mixing ratios (10−1,000 ppb), exceeding those in outdoor forested environments. The emitted terpenes react with indoor atmospheric O_3 and initiate indoor NPF, resulting in nucleation rates as high as ∼10^5 cm^{-3} s^{-1} and condensational growth rates up to 300 nm h^{-1}; these are orders of magnitude higher than those reported during outdoor NPF events. Notably, high particle nucleation rates significantly increase indoor atmospheric NCA concentrations (10^5−10^8 cm^{-3}), and high growth rates drive their survival and growth to sizes that efficiently reach the deepest regions of the human respiratory system. We found sVCP-nucleated NCA to cause respiratory exposures and dose rates comparable to or exceeding those from primary aerosol sources such as gas stoves and diesel engines, highlighting their significant impact on indoor atmospheric environments.

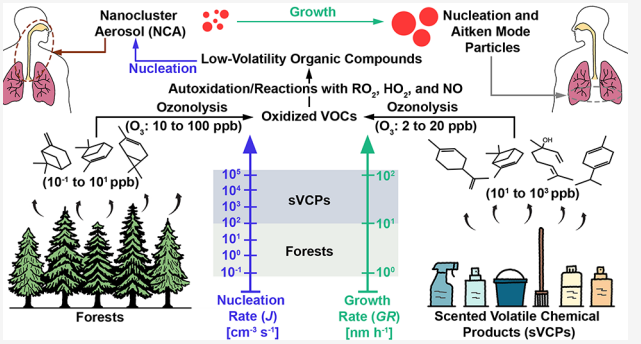

KEYWORDS: *indoor air quality, new particle formation (NPF), ultrafine particles, indoor atmospheric chemistry, volatile organic compounds*

INTRODUCTION

Volatile chemical products (VCPs), ubiquitous in the home environment, have the potential to replicate the complex biogenic reactive chemistry of dense forests within the enclosed spaces of our homes, offices, and schools. Emissions of volatile organic compounds (VOCs) from VCPs rival those from traditional sources[1] and participate in photochemistry and ozonolysis to yield a broad spectrum of oxygenated VOCs (OVOCs) and secondary particles,[2−4] with both primary and secondary products known to cause detrimental human health effects.[5] Therefore, VCPs have been identified as a potential source of contaminants of emerging concern.[1,6,7] Fragrances, often terpenes such as monoterpenes, and their oxygen-containing derivatives, monoterpenoids, are commonly added to VCPs to elevate the user's olfactory experience during use.[8,9] Such scented VCPs (sVCPs) encompass a broad range of consumer products, including personal care products (PCPs), air fresheners and other aromatherapy products, laundry products, cleaning supplies, and disinfectants.[9,10] The widespread availability of sVCPs in major retail stores highlights their extensive use and accessibility. A national survey in the U.S. revealed that 98.3% of Americans encounter sVCPs weekly through personal use, and when including indirect interactions, this increases to 99.1%.[11] The global home fragrance market, valued at approximately 11.12 billion USD in 2023, is expected to continue to grow.[12] In the U.S. alone, fragranced consumer products contribute about 26 (±20) kilotons of monoterpenes to the outdoor environment annually.[6] Despite their extensive use, the role of sVCPs on air quality remains one of the most uncertain sources of air pollution in the U.S.[3]

Previous studies have explored various aspects of secondary particle formation from sVCPs, with notable findings that include reaction mechanisms,[8] molecular composition of gas-

Received: June 2, 2024
Revised: August 20, 2024
Accepted: August 21, 2024
Published: September 24, 2024

phase species,[13−16] and high mass-based particle formation yields.[3,4,16,17] However, these studies have often focused on either gas-phase components or larger particles, leaving a critical size fraction that bridges these scales undetected and uncharacterized. This size fraction includes the sub-3 nm nanocluster aerosol (NCA) regime, where gas-to-particle transition occurs,[18] and the early growth nanoparticle regime, known as the "valley of death",[19] where sub-10 nm particles with high Brownian diffusivities are likely to be lost due to coagulation scavenging. Studies reporting indoor NCA concentrations and characterizing their formation and growth dynamics are limited,[20−23] with no studies available for realistic sVCP use scenarios indoors. NCA are efficiently deposited in the upper human respiratory tract (deposition fraction (DF_{max}) ∼ 1 nm) and the tracheobronchial region (DF_{max} ∼ 4 nm).[2,24] If they survive their high Brownian diffusivities, they can grow to sizes that efficiently reach the pulmonary region (DF_{max} ∼ 30 nm).[2]

A host of laboratory chamber studies have revealed that monoterpenes and monoterpenoids can surpass the nucleation barrier and the "valley of death" upon oxidation.[25−34] However, it remains unclear whether these outcomes will persist in real-world sVCP use scenarios indoors, where the levels of both precursors and oxidants vary widely depending on the immediate environment and the product used. Additionally, the much larger surface area available indoors compared to laboratory chambers[35] and the presence of occupants introduce further complexities that may influence these outcomes. The abundance of surfaces indoors can serve as sinks, sources, or media for heterogeneous chemistry involving particles and reactive gases. Moreover, the indoor environment can be highly dynamic due to human activities and occupancy patterns, which can alter ventilation rates and result in indoor oxidant concentrations being only a fraction of those found outdoors. Furthermore, human occupants can also act as sinks for oxidants such as O_3 due to the presence of skin oils.[22] Occupants also introduce a variety of sVCPs in their daily activities, with varying fragrances that may result in high concentrations of reactive gases indoors. Therefore, it is important to understand the fate of these uncharacterized nanoparticles during real-world sVCP use scenarios indoors, particularly since sVCP usage typically occurs in the presence of occupants. This knowledge gap exists due to the analytical challenges in measuring nanoparticles in real-time at the molecular scale.[36] However, recent progress in measurement techniques for sub-10 nm particles based on high-resolution electrical mobility classification, combined with advances in particle magnifying methods and material balance modeling of indoor nanoparticle dynamics, has facilitated the precise sizing, detection, and modeling of clusters down to approximately 1 nm.[20,37]

Here, we present the first comprehensive evaluation of new particle formation (NPF; secondary NCA nucleation and subsequent growth) during the use of sVCPs in a full-scale, mechanically ventilated residential test house, integrating measurements from a novel high-resolution particle size magnifier−scanning mobility particle sizer (PSMPS)[20] and a proton transfer reaction time-of-flight mass spectrometer (PTR-TOF-MS). We quantitatively show that the use of sVCPs can drive extremely rapid changes in indoor atmospheric nanoparticle concentrations at comparatively low O_3 mixing ratios with unprecedented NCA nucleation and growth rates that far exceed those observed during outdoor NPF events. Consequently, sVCP use can result in a high respiratory burden to all regions of the human respiratory system. Our measurements are unique in that they fuse advanced instrumentation with a comprehensive physics-based aerosol dynamics model, allowing for fundamental size- and time-scale evaluations of sVCP-nucleated indoor atmospheric NCA dynamics. This study is the first reporting of NCA nucleation rates and their subsequent growth rates for indoor terpene ozonolysis. It accurately models coagulation for the first time as both a loss ($CoagSnk_{d_p}$) and source term ($CoagSrc_{d_p}$), along with corrected condensational growth rates for indoor NPF. Such comprehensive characterization bridges the gap between gas-phase and larger particle measurements, allowing for the parametrization of nanoparticle source strength from sVCP usage. This advances a key step forward in understanding how sVCP use influences indoor air quality and human health.

MATERIALS AND METHODS

Field Measurement Site. Field measurements of NCA formation and growth during the use of sVCPs for common household activities were conducted in a single-zone mechanically ventilated residential building: the Purdue zero Energy Design Guidance for Engineers (zEDGE) test house. The test house has been described in detail elsewhere.[13,15,20,38−41] Four indoor mixing fans were installed in the test house to facilitate indoor air mixing. The mixing state of the test house for both particles and VOCs has been empirically validated.[15,20] The particle- and gas-phase constituents of the test house were continuously monitored in real-time by using a suite of advanced instrumentation, as detailed in the Measurements section. Figure S1 illustrates the layout of the test house and the locations of the instruments during the field measurement campaign.

sVCP Use Activities in the Purdue zEDGE Test House. We conducted controlled activities to realistically simulate specific, isolated, common household activities involving the use of terpene-rich sVCPs for floor mopping, aromatherapy, and self-care purposes. For the mopping activities, triplicate indoor floor mopping activities were performed by using a popular terpene-rich cleaning solution. For aromatherapy, six activities were conducted in total, including triplicate activities involving the spraying of a citrus-scented air freshener in the test house and three activities using essential oil diffusers with three different blends of essential oils: bergamot, citrus, and thieves. For self-care regimes, three activities were conducted using spray-based PCPs. Additionally, triplicate citrus fruit peeling activities were conducted inside the test house to serve as a reference for indoor terpene source events.[42,43] In total, 15 indoor sVCP use activities were conducted. Throughout the field measurement campaign, volunteers were instructed not to apply any PCPs except during PCP use activities.

The sequence for each category of activity—terpene mopping ($n = 3$), essential oil diffuser ($n = 3$), citrus-scented air freshener ($n = 3$), PCPs ($n = 3$), and citrus fruit peeling ($n = 3$)—is detailed in the Supporting Information (SI). Briefly, each activity consisted of three distinct periods: the background period (B), the source event period (S), and the decay period (D). The outdoor air ventilation rate was maintained at a nominal rate of 6.3 h^{-1} throughout all three periods, facilitating the introduction of ambient O_3 into the test house. After the decay period, the indoor air was purged with an outdoor air ventilation rate of 9 h^{-1} for at least 30 min. Each activity commenced with two volunteers entering the test house at time zero. The initial ten minutes of the activity served as the background period, during which the test house remained

https://doi.org/10.1021/acsestair.4c00118
ACS EST Air 2024, 1, 1276−1293

inactive to establish a baseline concentration of indoor air pollutants with people present. Following this, the terpene-rich sVCP was introduced, marking the beginning of the source period. We then observed the evolution of gas- and particle-phase constituents in the test house for 1 h after the end of the source period. All sVCPs used in these activities are readily available in major big-box retail stores in the U.S.

Measurements. *Online Nanoparticle Measurements.* Indoor atmospheric nanoparticle number concentrations and size distributions from 1.2 to 572.5 nm were measured in real-time using two different aerosol instruments: a novel particle size magnifier−scanning mobility particle sizer (PSMPS; GRIMM Aerosol Technik Ainring GmbH & Co. KG, Ainring, Germany)[20] and a SMPS with a long differential mobility analyzer (DMA) (Model 3938NL88, TSI Inc., Shoreview, MN, U.S.).[44,45] The PSMPS features a diethylene glycol-based particle size magnifier (PSM; Model A10, Airmodus Ltd., Helsinki, Finland) and a modified Vienna-type short DMA, facilitating high-size- and time-resolved NCA detection and classification. Additional details on the configuration and setup of the instruments can be found in Patra et al.[20] and are summarized in the SI. The PSMPS and SMPS measured particle number size distributions ($dN/d\log D_p$; cm^{-3}) for particles ranging from 1.2 to 55.7 nm and 13.1 to 572.5 nm in electrical mobility diameter, respectively, with a 2 min DMA scan interval. Since the PSMPS classifies particles by electrical mobility using a soft X-ray neutralizer, the electric charge may interact with carrier gas molecules during this process to produce charger ions in the NCA size fraction (1.2 nm < d_p < 3 nm). Therefore, the particle number size distributions from the PSMPS in the NCA size range were corrected for charger ions following the method proposed in Patra et al.,[20] with minor modifications (as detailed in the SI). Corrections were also made for diffusional losses within the PSMPS instrument.

Particle number size distributions from the SMPS in the size range of 13.1 to 200 nm were used as provided by the data acquisition software from the manufacturer (Aerosol Instrument Manager, TSI Inc., Shoreview, Minnesota, U.S.) without modifications. Due to the operational limitations of the SMPS,[46−49] particle number size distributions from 200 to 572.5 nm were corrected using a monotonic cubic spline interpolation.[50] This method ensures smooth and accurate fitting across the specified size range, effectively addressing gaps or inconsistencies in the data while preserving the shape of the particle number size distribution. Finally, the particle number size distributions from PSMPS and SMPS in the overlapping size range were merged using a moving average smoothing approach to obtain a continuous particle number size distribution from 1.2 to 572.5 nm. In the overlapping size range (13.1 to 55.7 nm), we took the mean values at the same d_p from the two instruments. At the edges of the overlap, we applied a moving average with a window size of 7 (three previous points, three subsequent points, and the current point) for smoothing. The measured particle number size distributions from the PSMPS were size-integrated from 1.2 to 3 nm to derive size-integrated NCA number concentrations (N_{NCA}; cm^{-3}).

Online Gas-Phase Measurements. Indoor atmospheric VOC mixing ratios were measured in real-time (1 Hz) by a proton transfer reaction time-of-flight mass spectrometer (PTR-TOF-MS; PTR-TOF 4000, Ionicon Analytik GmbH, Innsbruck, Austria).[15,38,41] The hydronium ion (H_3O^+) was used as the reagent ion, which ionized the sampled VOC molecules that have proton affinities greater than water, converting them into protonated molecules ($VOCH^+$) via a proton transfer reaction in the drift tube.[51,52] These protonated molecules were then separated and detected by the TOF-MS. Mass-to-charge ratios (m/z) from 30 to 450 were recorded. Additional configuration details of the PTR-TOF-MS used in this study are discussed in the SI. In this study, we are interested in the mixing ratios of monoterpenes ($C_{10}H_{16}$) and monoterpenoids ($C_{10}H_{14}O$, $C_{10}H_{16}O$, $C_{10}H_{18}O$, and $C_{10}H_{20}O$) detected at nominal m/z values of 81, 137, 151, 153, 155, and 157. These values represent a fragment $[C_6H_9]^+$, and the protonated masses of $[C_{10}H_{17}]^+$, $[C_{10}H_{15}O]^+$, $[C_{10}H_{17}O]^+$, $[C_{10}H_{19}O]^+$, and $[C_{10}H_{21}O]^+$, respectively. Table S1 provides the precise m/z values and identifies possible isomers for each chemical formula.

The PTR-TOF-MS was calibrated daily using two gas standards,[13,15] and the mixing ratios of VOCs not available in the gas standards were calculated using the Ionicon Data Analyzer (IDA) software (Ionicon Analytik GmbH, Innsbruck, Austria),[13] as detailed in the SI. The total terpene mixing ratios are expressed as the sum of the mixing ratios for monoterpenes and monoterpenoids (MT+MTD) at nominal m/z values of 81, 137, 151, 153, 155, and 157, where the reported mixing ratios for each m/z value represent the sum of all isomers sharing the same chemical formula. This was done due to the poorly characterized fragmentation patterns of monoterpenoids,[13] and because the PTR-TOF-MS lacked a fast gas chromatograph (GC) module at the inlet to separate isomers.[53] The approximate compositions of the monoterpene and monoterpenoid isomers in the sVCPs used in this study are summarized in Table S2, which also lists the second-order ozonolysis rate constants for the constituent isomers. A composition-weighted ozonolysis rate constant was determined for each sVCP, using the isomer composition and their respective second-order ozonolysis rate constants, to represent the effective isomer-weighted terpene ozonolysis rate constant (K_{eff}; $cm^3\ s^{-1}$).[54,55] Other trace gas instrumentation used during the field measurement campaign included NO_x ($NO + NO_2$), O_3, CO_2, and SO_2 analyzers (as detailed in the SI). Data from the gas-phase measurement equipment were aggregated and averaged every two minutes to align with the DMA scan interval of the PSMPS and SMPS.

Indoor Atmospheric NCA Dynamics Modeling. Atmospheric NPF events are typically characterized using two key parameters: the particle nucleation rate (J; $cm^{-3}\ s^{-1}$) and the particle growth rate (GR; nm h^{-1}).[56] The former parameter indicates the rate at which particles of a specific diameter are formed, while the latter quantifies how rapidly these particles grow to larger sizes. Within the NCA size fraction (1.2 nm < d_p < 3 nm), the measured concentrations in the 1.2−1.7 nm range can include very small particles, large gas molecules, and molecular clusters.[57,58] The distinction between these cannot be made using PSMPS measurements.[57] Therefore, the nucleation rate is usually determined at the critical diameter, representing the size at which a particle is considered to be stable against evaporation.[59] This diameter is approximately 1200 Da or ∼1.7 nm in electrical mobility diameter for NPF events.[28,60] Thus, in this study, we calculated the indoor atmospheric NCA nucleation rate at 1.75 nm ($J_{1.75}$; $cm^{-3}\ s^{-1}$) as characterized by the PSMPS bin having lower and upper size limits of 1.7 and 1.8 nm, respectively. $J_{1.75}$ is calculated as the net growth flux across this bin, using the discrete aerosol general dynamics equation (GDE) in a Eulerian specification (as shown in eq 1).[20,59]

https://doi.org/10.1021/acsestair.4c00118
ACS EST Air 2024, 1, 1276−1293

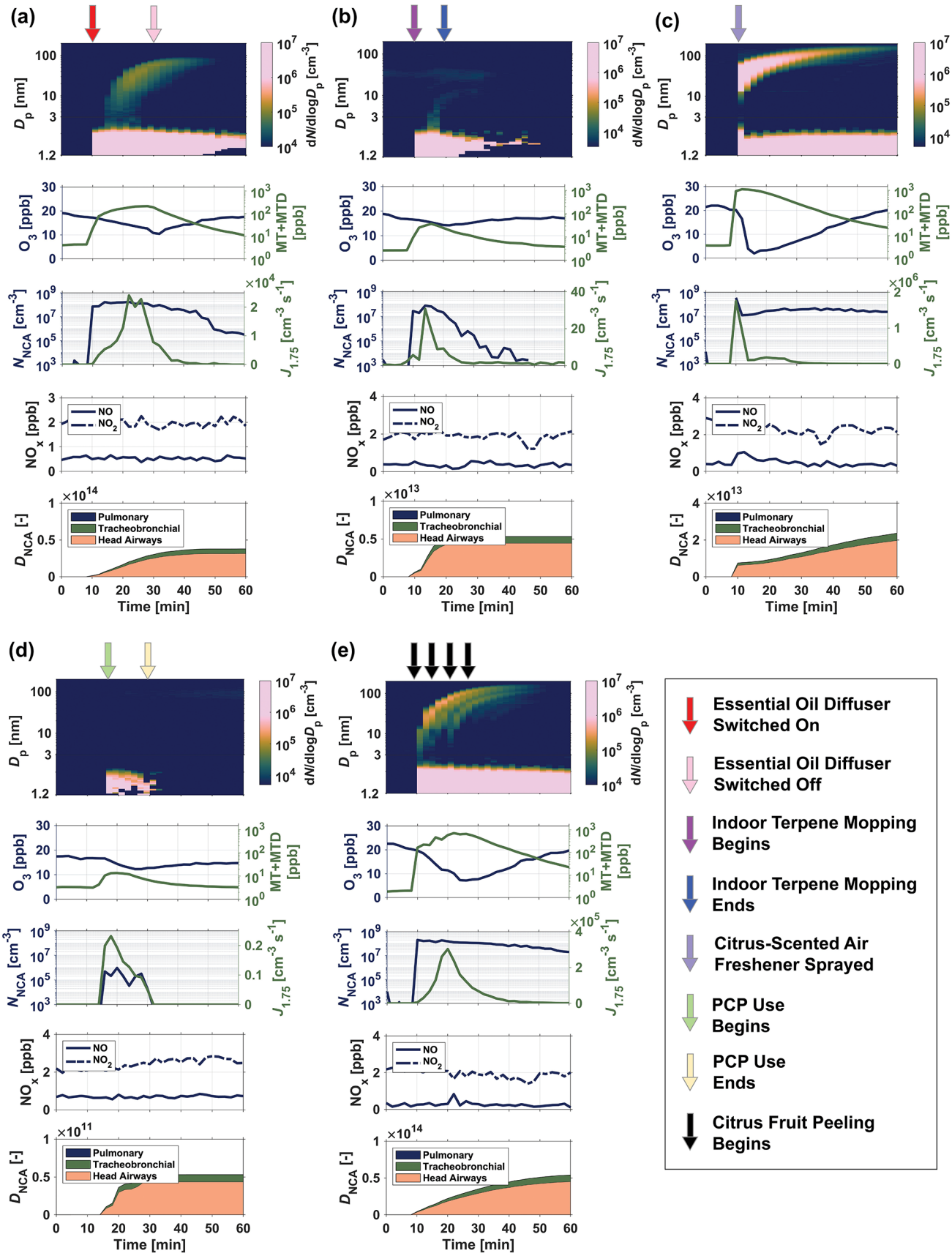

Figure 1. Time-resolved evaluation of indoor atmospheric nanoparticle nucleation and growth (new particle formation (NPF))—first row: particle number size distributions ($dN/d\log D_p$) from 1.2 to 200 nm; second row: mixing ratios of indoor atmospheric O_3 (blue line, left *y*-axis) and terpenes (expressed as the sum of mixing ratios of monoterpenes and monoterpenoids; green line, right *y*-axis); third row: size-integrated (1.2−3 nm) sVCP-

https://doi.org/10.1021/acsestair.4c00118
ACS EST Air 2024, 1, 1276−1293

Figure 1. continued

nucleated NCA number concentrations (N_{NCA}; blue line, left *y*-axis) and particle nucleation rates at 1.75 nm ($J_{1.75}$; green line, right *y*-axis); forth row: mixing ratios of indoor atmospheric NO (solid blue line) and NO_2 (dashed blue line); and fifth row: cumulative adult respiratory tract deposited doses (D_{NCA})—during representative indoor sVCP use activities (a: using an essential oil diffuser; b: mopping using a terpene-rich cleaning agent; c: using a citrus-scented air freshener; d: applying a PCP; and e: peeling citrus fruits (reference terpene source)) in the Purdue zEDGE test house. The temporal evolution of indoor atmospheric nanoparticles, terpenes, and O_3 for all sVCP use activities is provided in the SI (Figures S4−S8). Note: the color bar for particle number size distributions from 10^6 to 10^7 cm^{-3} is represented by a single color.

$$J_{1.75} = \left(\frac{dN_{1.75-u}}{dt} + \sum_{d_p=1.75}^{u} k_{vent} \cdot N_{d_{p,i}} + \sum_{d_p=1.75}^{u} k_{dep,d_p} \cdot N_{d_{p,i}} + \sum_{d_p=1.75}^{u} CoagSnk_{d_p} \cdot N_{d_{p,i}} - \sum_{d_p=1.75}^{u} CoagSrc_{d_p} + C_u \cdot N_{u,i} \right) \quad (1)$$

The subscript u corresponds to the upper bound of the size range used in the aerosol GDE for the estimation of $J_{1.75}$. Kulmala et al.[61] recommended the upper bound size to be the maximum size the critical cluster can reach during a short growth time interval. Therefore, in our analysis, we utilized an event-specific upper bound that corresponds to the maximum size identified by our growth rate determination algorithm (Figure S3).

The first term on the RHS of eq 1 represents the time rate of change in particle number concentrations from 1.75 nm to the upper bound size. The second term on the RHS of eq 1 accounts for particle loss due to ventilation, where k_{vent} is the nominal outdoor air ventilation rate (s^{-1}). $N_{d_{p,i}}$ corresponds to the indoor particle number concentration at size d_p, as characterized by the PSMPS bin i with a midpoint diameter d_p (cm^{-3}). The third term on the RHS of eq 1 describes particle loss due to deposition onto indoor surfaces due to Brownian and turbulent diffusion, where k_{dep,d_p} is the size-dependent first-order deposition loss rate coefficient for particles at size d_p (s^{-1}). k_{dep,d_p} was estimated using an indoor particle deposition model,[62] as detailed in Patra et al.[20] The fourth term on the RHS of eq 1 represents particle loss due to coagulation, where $CoagSnk_{d_p}$ is the coagulation sink for particles at size d_p (s^{-1}), expressed as shown in eq 2.[63]

$$CoagSnk_{d_p} = \sum_{d'_p=1.2nm}^{d'_p=572.5nm} k_{coag}(d_p, d'_p) \cdot N_{d'_{p,i}} \quad (2)$$

In eq 2, $k_{coag}(d_p, d'_p)$ represents the coagulation coefficient between particles at sizes d_p and d'_p (cm^3 s^{-1}). $N_{d'_{p,i}}$ is the particle number concentration in size bin i with the midpoint diameter d'_p. The coagulation coefficient $k_{coag}(d_p, d'_p)$ is calculated using the Brownian and van der Waals viscous forces coagulation model.[64] The Hamaker constant used in the coagulation model is 9×10^{-20} J, as experimentally determined by Cai et al.[65] for oxidized organic particles formed through nucleation initiated by limonene ozonolysis at 20 °C. This is pertinent because it represents particles similar to those studied here, maintained at the same nominal temperature. The fifth term on the RHS of eq 1 quantifies the formation of particles from the coagulation of smaller particles, expressed as $CoagSrc_{d_p}$ (as shown in eq 3) (cm^{-3} s^{-1}).[66]

$$CoagSrc_{d_p} = \sum_{d_p^3 = d'^3_p + d''^3_p}^{d'_p, d''_p < d_p} 0.5 \cdot k_{coag}(d'_p, d''_p) \cdot N_{d'_{p,i}} \cdot N_{d''_{p,j}} \quad (3)$$

In eq 3, d'_p and d''_p represent particles with sizes smaller than d_p, which coagulate to form particles of the size d_p. $N_{d'_{p,i}}$ and $N_{d''_{p,j}}$ are the corresponding particle number concentrations in size bins i and j, with midpoint diameters d'_p and d''_p, respectively. The exclusion of $CoagSrc_{d_p}$ when modeling NCA dynamics can introduce uncertainties in estimating nucleation rates, often resulting in overestimation.[20] Additionally, it is important to note that $CoagSrc_{d_p}$ has not been previously modeled in the context of indoor NCA formation from precursor VOCs.

The final term on the RHS of eq 1 represents the outbound condensational flux at the upper bound size, where $N_{u,i}$ is the particle number concentration in size bin i with midpoint diameter u, and C_u is expressed as shown in eq 4 (s^{-1} or h^{-1}).[67]

$$C_u = \frac{GR_u}{\Delta u} \quad (4)$$

In eq 4, GR_u is the net condensational growth rate at the upper bound size u, and Δu is the width of the upper bound size bin. The net condensational growth rate (GR_{Cond,d_p}; nm h^{-1}) is calculated using the mode-fitting method[68] and is corrected for growth due to intramodal coagulation[66] (GR_{Coag,d_p}; nm h^{-1}) and intermodal coagulation[69] (GR_{Scav,d_p}; nm h^{-1}). A detailed explanation of the various growth rates can be found elsewhere.[70] The mode-fitting method and different growth rates obtained for a representative activity are shown in Figures S3 and 6(a), respectively.

Overall, eq 1 represents a material balance equation over the entire indoor nanoparticle population related to nucleation and growth processes. The condensational flux appears only at the upper bound size because the condensational sources and losses offset each other at the individual bin level.[59] A detailed derivation of eq 1 can be found in Cai et al.[59] It is important to note that eq 1 models coagulation as both a source and a loss term, and the condensational flux is calculated by correcting the growth rates for intermodal and intramodal coagulation to obtain the corrected net condensational growth rates (GR_{Cond,d_p}). This is crucial for accurate modeling of NCA nucleation rates, which have previously been ignored in ultrafine and nanoparticle modeling studies. Additionally, based on methods outlined in prior studies,[20,41,71] we also estimated the respiratory tract deposited dose rates (R_D; min^{-1}) and cumulative respiratory tract deposited doses to evaluate the rate of deposition and total deposition of secondary nanoparticles formed during indoor sVCP use in different respiratory tract regions (head airways, tracheobronchial, pulmonary) of adults (as detailed in the SI).

https://doi.org/10.1021/acsestair.4c00118
ACS EST Air 2024, 1, 1276−1293

Table 1. Summary of sVCP Use Activities in the Purdue zEDGE Test House[a]

Source	ID	Mean		Outdoor Air Ventilation Rate [h^{-1}]	Mean Background Mixing Ratio [ppb]			Peak MT+MTD Mixing Ratio [ppb]	Mean GR_{Cond} [nm h^{-1}]			Median Background $CoagSnk_{1.75}$ [s^{-1}]	Median $J_{1.75}$ [cm^{-3} s^{-1}]
		T [°C]	RH [%]		NO + NO_2	O_3	SO_2 (Outdoor)		3–10 nm	10–25 nm	>25 nm		
Essential Oil Diffuser	1A	17.9	64.1	6.2	0.6 + 1.9	18.2	0.4	214.2	63.9	175.5	270.8	1.4×10^{-3}	1.3×10^{4}
	1B	17.4	61.4	6.2	0.5 + 1.9	19.1	0.5	387.5	CND	217.3	277.1	1.6×10^{-3}	6.6×10^{4}
	1C	17.4	63.4	6.2	0.5 + 1.7	16.5	0.3	133.8	31.2	119.2	167.9	8.0×10^{-4}	1.3×10^{3}
Indoor Terpene Mopping	2A	22.7	59.0	6.3	0.4 + 2.3	24.7	0.6	35.6	51.9	83.6	No Growth	1.5×10^{-3}	30.3
	2B	22.7	57.5	6.3	0.4 + 2.0	17.7	0.4	37.1	23.9	66.9	No Growth	1.3×10^{-3}	25.0
	2C	22.4	58.0	6.3	0.4 + 1.8	19.9	0.4	33.4	17.4	48.3	No Growth	1.6×10^{-3}	26.3
Citrus-Scented Air Freshener	3A	20.5	61.0	6.5	0.5 + 3.9	21.5	0.5	1128.7	CND	CND	307.4	1.7×10^{-3}	1.6×10^{5}
	3B	20.3	59.9	6.5	0.4 + 2.6	24.3	0.4	1119.3	CND	CND	300.3	1.4×10^{-3}	1.5×10^{5}
	3C	18.1	73.8	6.5	0.5 + 2.7	15.7	0.3	1411.1	CND	CND	307.1	1.0×10^{-3}	1.3×10^{5}
Personal Care Products (PCPs)	4A	17.9	67.5	6.8	0.6 + 2.6	20.8	0.4	151.9	No Growth	No Growth	No Growth	2.0×10^{-3}	2.5
	4B	18.2	76.9	6.3	0.7 + 2.0	17.2	0.1	13.6	No Growth	No Growth	No Growth	2.0×10^{-3}	0.7
	4C	18.1	76.7	6.5	0.7 + 2.0	17.3	0.1	3.9	No Growth	No Growth	No Growth	1.4×10^{-3}	No Nucleation
Citrus Fruit Peeling (Reference)	5A	19.0	68.7	6.1	0.2 + 2.0	21.6	0.2	717.2	CND	233.1	298.1	1.5×10^{-3}	1.5×10^{5}
	5B	18.9	69.0	6.1	0.3 + 2.4	22.2	0.2	638.9	141.8	209.4	293.1	2.2×10^{-3}	1.3×10^{5}
	5C	18.7	69.1	6.1	0.2 + 2.4	22.3	0.4	713.8	CND	240.4	311.3	1.9×10^{-3}	2.1×10^{5}

[a]CND: could not detect; constrained by the limitation of the mode-fitting growth rate determination algorithm due to the lack of a well-defined particle mode for smaller particle sizes.[70]

https://doi.org/10.1021/acsestair.4c00118
ACS EST Air 2024, 1, 1276−1293

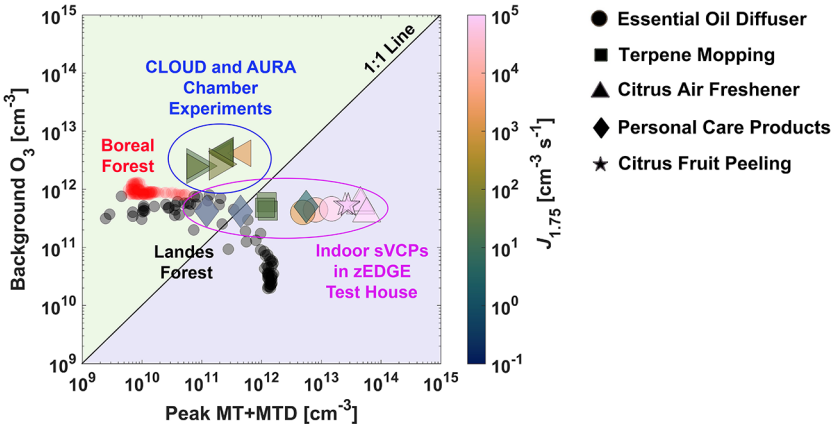

Figure 2. Relationship between the background indoor atmospheric O_3 mixing ratios and the peak cumulative monoterpene and monoterpenoid mixing ratios during indoor sVCP use activities. The source data for chamber experiments comes from Caudillo et al.[31] (CLOUD) and Thomsen et al.[25] (AURA). The mixing ratios represent the initial concentrations of O_3 and terpenes used in the chamber experiments. The source data for Boreal and Landes forests come from Li et al.[73] The mixing ratios represent the diurnal concentrations of O_3 and terpenes in the forest. The data points for indoor sVCP and chamber experiments are color coded by the particle nucleation rates ($J_{1.75}$ for our study, and $J_{1.7}$ for chamber experiments).

RESULTS AND DISCUSSION

Indoor Atmospheric Chemistry during Indoor sVCP Use. Figure 1 presents the time-resolved evaluation of indoor atmospheric NPF initiated by the use of different sVCPs in the test house. It also illustrates the direct emissions of terpenes to indoor air, measured by PTR-TOF-MS as cumulative signals detected for monoterpenes and monoterpenoids (MT+MTD). sVCP use results in significant emissions of terpenes. Manufacturers deliberately fragrance these products primarily to create pleasant indoor smellscapes,[9,10] but they also inadvertently become major sources of terpenes. The amount of terpenes released and their temporal emission profiles vary with the type of sVCP used (Figure 1). Activities such as mopping the floor using a terpene-rich cleaning agent, using citrus-scented air fresheners, and applying PCPs result in pulsed terpene emissions to indoor air, with terpene mixing ratios peaking within five minutes of source introduction (Figures 1, S4, S5, and S6). Conversely, using essential oil diffusers or peeling citrus fruits (reference terpene source) causes a more gradual increase in the terpene mixing ratios (Figures 1, S7, and S8). This is the first demonstration of diverse terpene emissions from a variety of different sVCPs during their realistic usage as observed via PTR-TOF-MS. The peak terpene mixing ratios during the use of essential oil diffusers, mopping using a terpene-rich cleaning agent, using citrus-scented air fresheners, applying PCPs, and peeling citrus fruits (reference terpene source) were 133−387 ppb, 33−37 ppb, 1128−1411 ppb, 4−151 ppb, and 638−717 ppb, respectively. Notably, a single spray of citrus-scented air freshener resulted in the highest terpene emissions, with peak emissions exceeding 1000 ppb (Figure 1 and Table 1). Terpene emissions from sVCPs are comparable to or higher than those reported in other indoor and outdoor environments (Table S3).[13,41,72−74]

Terpene emissions from sVCPs are predominantly composed of d-limonene (40−100%; Table S2). Other dominant terpenes included α-pinene and γ-terpinene. All these terpenes contain at least one endocyclic carbon double bond.[75−77] This functionality shows high reactivity toward O_3.[78,79] Hence, O_3 is seen to be consumed in the test house immediately after terpene emissions begin (Figure 1), initiating gas-phase ozonolysis. Monoterpene oxidation proceeds via the formation of peroxy radicals ($RO_2^\bullet$), which can react with NO, HO_2, or other peroxy radicals. However, under low NO conditions, the ozonolysis of endocyclic double bonds can initiate a rapid oxidation process called autoxidation that can compete with reactions with NO, HO_2, and other peroxy radicals.[80] Autoxidation is characterized by repeated intramolecular hydrogen shifts (H-shifts) in the weakly attached hydrogen atoms of peroxy radicals.[81] After each H-shift, molecular O_2 is quickly added, forming highly oxygenated peroxy radicals that retain their radical functionality but become more oxygen-rich. Not only the monoterpenes but also linalool ($C_{10}H_{18}O$), a monoterpenoid present in one sVCP we tested, can undergo $RO_2^\bullet$ and $RO^\bullet$ modulated autoxidation.[8] Notably, high $RO_2^\bullet$ concentrations (2 to 3 × 10^9 cm^{-3}) have previously been observed during indoor terpene ozonolysis events.[2] Through autoxidation, various highly oxygenated molecules (HOMs) are formed, covering a spectrum of volatilities from low-volatility organic compounds (LVOCs; 3 × 10^{-5} < c° < 0.3 $\mu g\ m^{-3}$) to extremely low-volatility organic compounds (ELVOCs; 3 × 10^{-9} < c° < 3 × 10^{-5} $\mu g\ m^{-3}$) to ultra low-volatility organic compounds (ULVOCs; c° < 3 × 10^{-9} $\mu g\ m^{-3}$).[30] Figure S9 presents a selection of key oxidized VOCs from d-limonene ozonolysis. In environments with low NO levels, the $RO_2^\bullet$ radicals terminate by engaging in radical−radical interactions that produce either monomers or covalently linked dimers (ROOR′) with ultra low-volatility.[26,30,82] These ULVOCs can nucleate to form new particles, playing a crucial role in biogenic NPF.[30]

Indoor environments have been found to facilitate bimolecular radical reactions through autoxidation when NO mixing ratios are below 0.8 ppb.[42] During our field measurement campaign, the NO levels were always less than 0.8 ppb for all sVCP use activities (Figure 1 and Table 1). Furthermore, high terpene emissions from sVCPs often resulted in terpene mixing ratios exceeding those of indoor O_3 levels (Figure 2). Prior to sVCP use, indoor O_3 levels ranged from 15 to 25 ppb, primarily introduced to the test house through mechanical ventilation, while terpene mixing ratios reached 10 to 1000 ppb during sVCP use. Such O_3-limited terpene ozonolysis reactions are shown to yield products with a higher nucleation potential.[83] Consequently, we see a burst of nucleation immediately after sVCPs were used. This is evidenced by the emergence of a large pool of freshly nucleated molecular clusters that significantly increase indoor atmospheric NCA levels, as shown in both the particle

https://doi.org/10.1021/acsestair.4c00118
ACS EST Air 2024, 1, 1276−1293

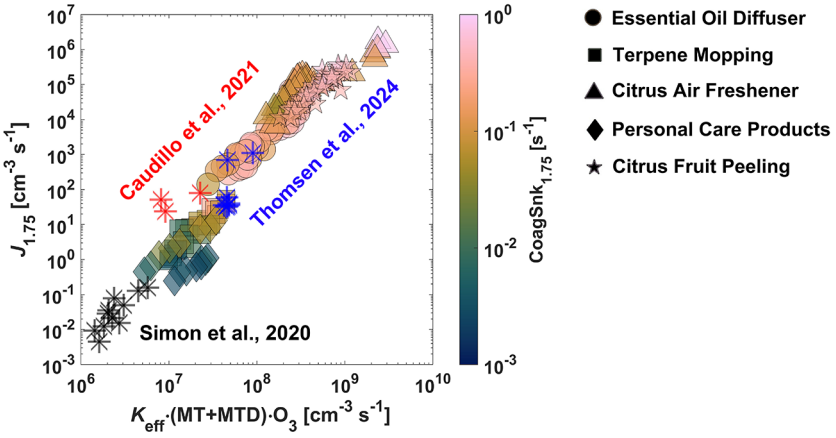

Figure 3. Relationship between the effective terpene ozonolysis reaction rates and particle nucleation rates at 1.75 nm ($J_{1.75}$) during indoor sVCP use activities. K_{eff}, a composition-weighted effective rate constant, is calculated using the isomer composition and their respective second-order ozonolysis rate constants. The closed symbols represent data from our study, while the open symbols represent data from the literature. Each closed symbol represents a data point obtained during indoor sVCP use activities from the initial introduction of the sVCP until the next 30 minutes, with measurements taken at 2-minute intervals. The symbols are color coded by the corresponding coagulation sink for 1.75 nm particles.

number size distributions and the size-integrated NCA number concentrations, N_{NCA} (Figure 1). N_{NCA} levels increased from background concentrations of approximately 10^2 cm^{-3} to >10^5 cm^{-3} within a few minutes after introducing sVCPs. Peak N_{NCA} concentrations were highest for activities using citrus-scented air fresheners (median peak ~2.7 × 10^8 cm^{-3}), followed by citrus fruit peeling activities (reference terpene source; median peak ~2.0 × 10^8 cm^{-3}), activities involving using essential oil diffusers (median peak ~1.7 × 10^8 cm^{-3}), and mopping activities using a terpene-rich cleaning agent (median peak ~7.4 × 10^7 cm^{-3}). The lowest N_{NCA} concentrations were observed in activities involving the use of PCPs (median peak ~9.5 × 10^5 cm^{-3}). This trend followed that of the precursor terpene mixing ratios. sVCP-nucleated NCA concentrations were comparable to or higher than NCA levels reported for other primary and secondary NCA sources across different environments (Table S4).[2,18,20−23,84−87]

Indoor NCA Nucleation and Growth Rates during sVCP-Initiated Rapid NPF Events. We estimated particle nucleation rates ($J_{1.75}$) of sVCP-initiated NPF events to quantify the rate at which new particles form against indoor-specific loss processes (eq 1). Extremely high $J_{1.75}$ values, reaching 10^5 cm^{-3} s^{-1}, were observed (Table 1). The median $J_{1.75}$ values during the use of essential oil diffusers, mopping with a terpene-rich cleaning agent, using citrus-scented air fresheners, applying PCPs, and peeling citrus fruits (reference terpene source) were 0.1−6.6 × 10^4 cm^{-3} s^{-1}, 25.0−30.3 cm^{-3} s^{-1}, 1.3−1.6 × 10^5 cm^{-3} s^{-1}, 0.7−2.5 cm^{-3} s^{-1}, and 1.3−2.1 × 10^5 cm^{-3} s^{-1}, respectively. We tested citrus fruit peeling activities in the test house because this reference terpene source has been previously evaluated in indoor environments.[42,43] We observed nucleation rates similar to those reported (~10^5 cm^{-3} s^{-1}) for citrus fruit peeling activities. Surprisingly, very high nucleation rates were observed for other indoor sVCP use activities, with peak nucleation rates from spraying a citrus-scented air freshener exceeding those of citrus fruit peeling activities.

The wide variability in $J_{1.75}$ can be explained by the variations in the effective terpene ozonolysis rates (K_{eff}·(MT+MTD)·O_3)[26,27] during the activities (Figure 3). Furthermore, these nucleation rates correlate well with previously published $J_{1.7}$ values and terpene ozonolysis reaction rates observed in CLOUD[26] and AURA[25] chambers for pure biogenic terpene ozonolysis-induced nucleation, suggesting that terpene ozonolysis is the likely pathway for nucleation induced by sVCPs, and the high terpene emissions from sVCPs explain the high nucleation rates. Another interesting aspect of sVCP-induced NPF is that for activities such as using essential oil diffusers, mopping, using citrus-scented air fresheners, and peeling citrus fruits (reference terpene source), we see sustained nucleation even after the active terpene source emission period ended. This occurs because, for such activities, the indoor terpene mixing ratios remain elevated after the end of the source period due to the high terpene emissions (Figure 1) and potential residual emissions from surface films, which continue to react with O_3 to nucleate particles. However, this was not the case for activities with low terpene emissions, such as PCP use. The only activity where new particles were not formed was for a PCP use activity where no significant terpene emissions occurred (peak MT +MTD mixing ratio ~4 ppb; Table 1 and Figure S6(b)). This further corroborates the fact that the precursor terpenes drive nucleation during sVCP use. The nucleation rates observed for sVCP use activities rival the kinetic limit of H_2SO_4 nucleation at high H_2SO_4 concentrations (10^7 to >10^8 cm^{-3})[30] and nucleation bursts in pristine coastal NPF events.[88] Another notable feature of sVCP-initiated nucleation is that very high $J_{1.75}$ values were observed even when the CoagSnk$_{1.75}$ values were high (0.001−1 s^{-1}). These results demonstrate the effectiveness and rapidity of indoor atmospheric nucleation bursts due to sVCP use.

The newly formed sVCP-nucleated NCA grew to larger particle sizes within a few minutes after the start of sVCP use. The maximum diameter of particle growth ($d_{p,max}$) depended on the type of sVCP used. For essential oil diffusers and mopping with a terpene-rich cleaning agent, $d_{p,max}$ ranged between 35−74 nm and between 9−13 nm, respectively. $d_{p,max}$ for both citrus-scented air fresheners and citrus fruit peeling activities (reference terpene source) was greater than 100 nm (~150 nm). Interestingly, the nucleated NCA did not grow to larger sizes during PCP use activities. These variations can be explained by the amount of terpenes released from the sVCP use activities (Figure 2). For instance, as we move toward the right in Figure 2, the peak terpene emissions released from the sVCP use activity increase. This suggests that PCP use activities had the lowest terpene emissions, followed by mopping with a terpene-rich cleaning agent and using an essential oil diffuser.

https://doi.org/10.1021/acsestair.4c00118
ACS EST Air 2024, 1, 1276−1293

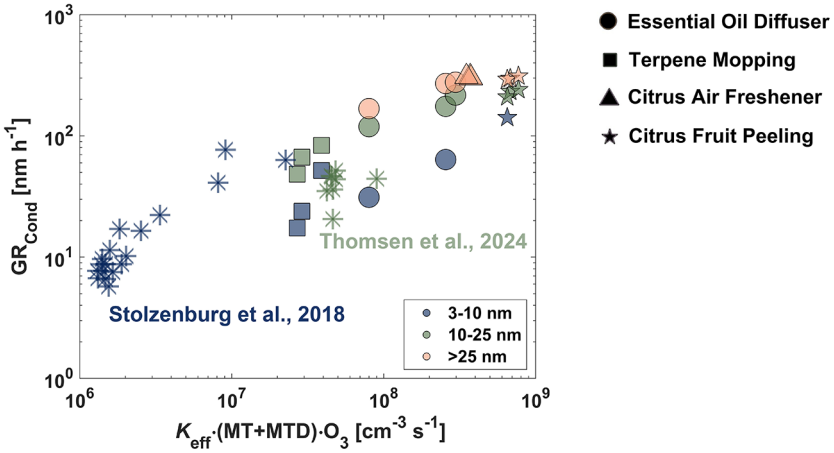

Figure 4. Relationship between the effective terpene ozonolysis reaction rates and net condensational growth rates (GR_{Cond}) during indoor sVCP use activities. K_{eff}, a composition-weighted effective rate constant, is calculated using the isomer composition and their respective second-order ozonolysis rate constants. The closed symbols represent data from our study, while the open symbols represent data from the literature. The data points are color coded by the size-interval used for the growth rate estimation. The GR_{Cond} in a specific size range represents the mean growth rate observed in that size interval.

The maximum terpene emissions were from using citrus-scented air fresheners and peeling citrus fruit. The $d_{p,max}$ for sVCP use activities, as noted previously, follows this trend. To quantify the rate at which the particles grew, we calculated the net condensational growth rates (GR_{Cond}) of the sVCP-nucleated NCA. GR_{Cond} were grouped into three size ranges: 3−10 nm, 10−25 nm, and 25−100 nm, and in each size fraction GR_{Cond} represented the mean GR_{Cond} observed in that specific size range. The lower size limit of GR_{Cond} for different sVCP use activities was constrained by the limitation of the mode-fitting growth rate determination algorithm due to the lack of a well-defined particle mode for smaller particle sizes.[70]

GR_{Cond} for sVCP use activities in the size ranges 3−10 nm, 10−25 nm, and 25−100 nm varied between 17−141 nm h^{-1}, 48−240 nm h^{-1}, and 168−312 nm h^{-1}, respectively. Thus, GR_{Cond} was observed to increase with an increasing particle size (Figure 4). This trend has been reported for NPF events from various regions across rural to urban polluted sites and is likely explained by the partitioning of additional semi-volatile vapors for larger particle sizes.[89−95] The variation in GR_{Cond} within different size fractions can be explained by variations in the effective terpene ozonolysis reaction rates during the activities (Figure 4). They also correlate well with observations in the CLOUD chamber for pure biogenic nucleation,[27] suggesting high terpene emissions from sVCPs also drive the high condensational growth rates. Therefore, the highest GR_{Cond} were observed during the use of citrus-scented air fresheners and peeling citrus fruit (reference terpene source), followed by using essential oil diffusers and mopping with a terpene-rich cleaning agent (Figure 4 and Table 1). The observed growth rates are an order of magnitude higher than the growth rates observed for outdoor atmospheric NPF events (∼1−10 nm h^{-1}).[70]

Differences in precursor terpene emission profiles for different sVCPs led to distinct indoor NPF events (Figure 1). The following types of NPF events were observed during sVCP use activities: *i.* no nucleation or particle growth (PCP use activity; Figure S6(b)); *ii.* nucleation but no particle growth (PCP use activities; Figures 1(d) and S6(a)); *iii.* nucleation and mild particle growth ($d_{p,max}$ < 20 nm; mopping with a terpene-rich cleaning agent; Figures 1(b) and S4); *iv.* nucleation and moderate particle growth (20 < $d_{p,max}$ < 100 nm; using essential oil diffusers; Figures 1(a) and S7); and *v.* nucleation and intense particle growth ($d_{p,max}$ > 100 nm; using citrus-scented air fresheners and peeling citrus activities (reference terpene source); Figures 1(c), 1(e), S5 and S8). Such diverse types of NPF have previously been identified for outdoor NPF events.[96,97] We are the first to document the diversity of indoor NPF types associated with the different sVCPs used in this study.

High GR_{Cond} is likely the reason NCA from sVCP use activities can overcome the "valley of death" region during periods of high terpene emissions. During these periods, the high condensational growth rates driven by high terpene emissions help prevent the loss of sub-10 nm particles due to coagulation scavenging.[19] Additionally, the newly formed NCA are subject to significant Kelvin curvature effects, and it is expected that these clusters initially grow through the condensation of extremely and ultra low-volatility organic compounds (ELVOCs and ULVOCs).[70,98,99] However, chamber studies on terpene oxidation[27] suggest that the highest concentrations of low-volatility gas-phase constituents remain in the LVOC region as they are formed during the initial stages of oxidation; more precursor VOCs are required to form ELVOCs and ULVOCs.[100] Consequently, not all freshly nucleated particles manage to grow beyond the NCA region, and they only grow when terpene emissions are high and approaching their peak (Figure 1).[101] For instance, during the PCP use activities, terpene emissions were not high, likely insufficient to form the significant ELVOCs and ULVOCs needed to overcome the Kelvin curvature effect. As a result, while terpene emissions from PCP use activities can nucleate NCA (albeit at a significantly lower nucleation rate compared to other sVCP use activities, as shown in Table 1), the particles do not grow beyond the NCA size regime (Figures 1(d) and S6). Similar nucleation events with no particle growth have been reported in outdoor environments, as illustrated in Figure 1 in Mazon et al.,[102] where the authors term them "quasi events". Other examples include Figure 3(b) in Yu et al.[103] and Figure 4(b) in Sebastian et al.[104] Furthermore, for other sVCP use activities, indoor NPF events initially exhibit nucleation and continuous growth as terpene emissions increase and approach their peak, followed by a period in which only NCA nucleation occurs without clear continuous

https://doi.org/10.1021/acsestair.4c00118
ACS EST Air 2024, 1, 1276−1293

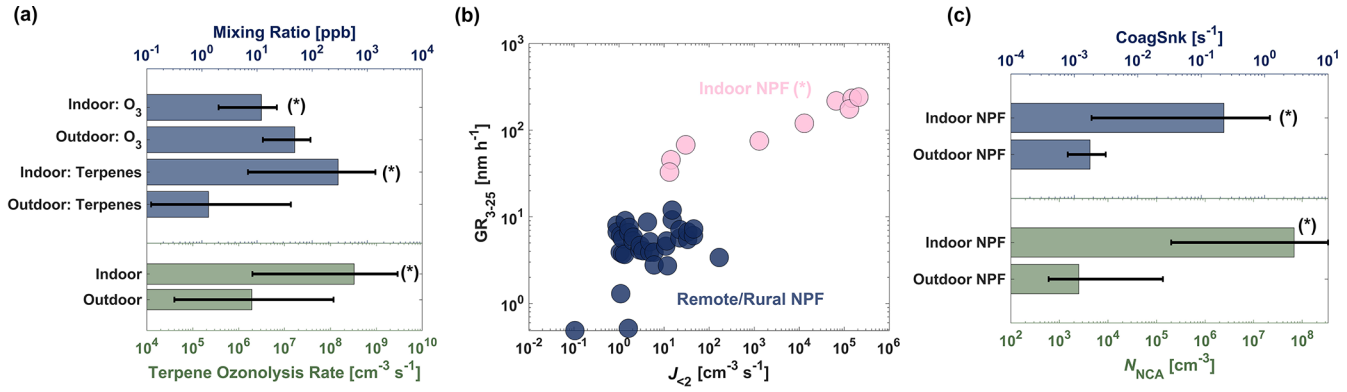

Figure 5. (a) Comparison between indoor and outdoor O_3 and terpene mixing ratios. The indoor O_3 and terpene mixing ratios are from this study during the NPF periods. The data for outdoor O_3 mixing ratio comes from Liao et al.,[128] and the data for outdoor terpene mixing ratio comes from Li et al.[73] The terpenes for this study include both monoterpenes and monoterpenoids; however, the outdoor terpenes only include monoterpenes. The indoor terpene ozonolysis rates were estimated using the indoor O_3 and terpene mixing ratios, and the composition-weighted effective ozonolysis rate constant (K_{eff}), calculated using the isomer composition and their respective second-order ozonolysis rate constants. The outdoor ozonolysis rates were estimated using the outdoor O_3 and terpene mixing ratios and an ozonolysis rate constant of 5×10^{-17} cm^3 s^{-1} (representing the average ozonolysis rate constant of α-pinene and β-pinene).[129] (b) Relationship between the particle nucleation rates for $d_p < 2$ nm particles and the mean growth rates of particles between 3 and 25 nm. The data points are color coded by the type of NPF events (blue: remote/rural NPF events; light pink: indoor NPF events (this study)). The data for remote/rural NPF come from a recent compiled review study on atmospheric nanoparticle growth rates.[70] (c) Comparison between indoor and outdoor size-integrated (1.2−3 nm for indoor NPF (this study) and 1.1−2.5 nm for outdoor NPF (Sulo et al.[57])) NCA number concentrations (N_{NCA}) and CoagSnk. The indoor CoagSnk is calculated for 1.75 nm particles (this study) and the outdoor CoagSnk is calculated for 1 nm particles in the boreal forest.[67] Both indoor N_{NCA} and CoagSnk were calculated during the indoor NPF periods. The error bars represent the minimum and maximum observed values in (a) and (c). (*) represents data from this study.

growth beyond the NCA size fraction as terpene emissions decline (Figure 1). Similar NCA persistence but no continuous growth has also been reported in both indoor and outdoor environments (Figure 2(e) in Rosales et al.,[2] Figure 8(f) in Baalbaki et al.,[105] Figure 4(a) in Sebastian et al.[104] and Figure 1(d) in Dada et al.[106]). To fully comprehend indoor atmospheric nanoparticle growth, future studies are needed to measure low-volatility condensable vapors using various high-resolution chemical ionization mass spectrometers during sVCP use activities.

To quantify the survival of particles beyond 3 nm during continuous growth periods of sVCP-initiated NPF events, we calculated the survival probabilities ($P_{d_1 \to d_2}$) of indoor atmospheric nanoparticles from 1.75 to 10 nm during sVCP use activities (as detailed in the SI). Median $P_{d_{1.75} \to d_{10}}$ for indoor sVCP use activities ranged from 5.6×10^{-4} to 2.6×10^{-1} (mean = 4.5×10^{-2}, Table S5). This is consistent with modeled calculations for an indoor environment, where authors reported that only 2% of the condensable gases condense onto particles while the rest are lost to surfaces and ventilation.[107] The variability in $P_{d_{1.75} \to d_{10}}$ during different sVCP use activities can be explained by the resulting coagulation sink and condensational growth rate ratio (Table S5). In urban polluted environments, $P_{d_{1.5} \to d_{10}}$ is typically reported to range between 10^{-5} to 10^{-2}.[63] Indoor sVCP use activities have higher survival probabilities than outdoor environments, presumably due to higher terpene emissions during sVCP use.

Another important thing to note is that particle growth due to coagulation (GR_{Coag}) can be significant for sub-10 nm particles during intense NPF events as observed here (Figure 6(a)). To quantify, for our sVCP use activities, GR_{Cond} can be overestimated by a median of 73%, 25%, and 10% in the size ranges 3−10 nm, 10−25 nm, and 25−100 nm, respectively, if the growth rates from the mode-fitting method are not corrected for growth due to coagulation (GR_{Coag} and GR_{Scav}) (Table S6). Such corrections have typically been overlooked in NPF studies. However, to model the net condensational growth rates correctly, coagulation must be accurately modeled and accounted for. Similarly, CoagSrc is often ignored while modeling indoor nanoparticle dynamics. Notably, our sVCP use activities suggest that CoagSrc can contribute between 40 and 49% to the estimated $J_{1.75}$ values (estimated as discussed in eq S2).

Comparison with Outdoor Atmospheric NPF and NCA Studies. NPF from terpene oxidation is extensively documented in outdoor environments.[108] These VOCs are also responsible for indoor NPF resulting from sVCP use activities. However, in contrast to outdoor terpene levels from terrestrial vegetation, sVCPs introduce significantly higher terpene mixing ratios into the indoor environment (Figure 5(a) and Table S3). Another difference between indoor and outdoor NPF is that indoor NPF typically occurs in an O_3-limited region, whereas outdoor NPF typically occurs in a terpene-limited region (Figure 2). Prior CLOUD and AURA chamber experiments on terpene ozonolysis usually simulate outdoor-relevant mixing ratios and thus also fall in the terpene-limited region (Figure 2). Thus, indoor NPF occurs at O_3 mixing ratios lower than outdoor environments and the studied chamber experiments.

Although indoor O_3 levels are lower, the high terpene emissions from sVCPs drive the indoor terpene ozonolysis rate (K_{eff}(MT+MTD)·O_3) to be 100 times higher than the outdoor rate (Figure 5(a)). The high indoor terpene ozonolysis rates and conditions favoring autoxidation[42] are likely the reason for very rapid indoor atmospheric NCA nucleation and growth (Figures 3, 4, and 5(b)). This study marks the first instance of characterizing the intensity of sVCP-initiated NPF in a real household setting through the parametrization of $J_{1.75}$ and GR_{Cond}. Such characterization is more advantageous than commonly used secondary organic aerosol yields as it provides a basis for understanding the intensity of NPF events and facilitates a direct comparison of NPF across different

https://doi.org/10.1021/acsestair.4c00118
ACS EST Air 2024, 1, 1276−1293

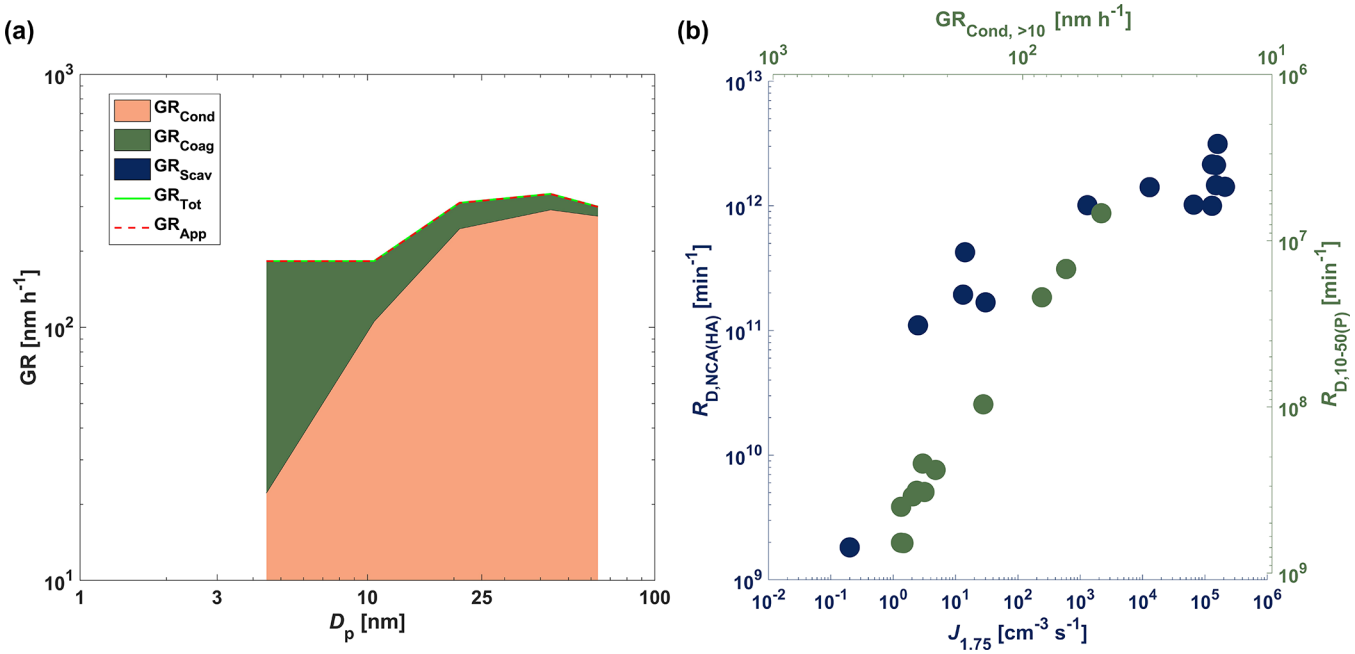

Figure 6. (a) Size-resolved growth rates (condensational growth rate (GR_{Cond}), intramodal coagulation growth rate (GR_{Coag}), intermodal coagulation growth rate (GR_{Scav}), total growth rate ($GR_{Tot} = GR_{Cond} + GR_{Coag}$), apparent growth rate ($GR_{App} = GR_{Cond} + GR_{Coag} + GR_{Scav}$)) for a representative essential oil diffuser use activity. (b) Relationship between (bottom *x*-axis) particle nucleation rates at 1.75 nm and (left *y*-axis) the rate of deposition of NCA in the adult human head airway region; and between (top *x*-axis) the condensational growth rate for particles greater than 10 nm and (right *y*-axis) the rate of deposition of 10−50 nm particles in the adult human pulmonary region during the indoor sVCP use activities. The data points are color-matched to their corresponding axes. The deposition and nucleation rates shown in the figure represent the median rates during the NPF period and the growth rates represent the mean growth rate of particles greater than 10 nm for each sVCP use activity (a similar analysis is shown in Figure S11, with the *x*-axes representing size-integrated indoor atmospheric NCA and 10−50 nm nanoparticle concentrations).

environments. When compared with outdoor remote NPF events, which are primarily driven by biogenic emissions, sVCP-initiated indoor atmospheric NPF can reach nucleation rates up to 10,000 times faster for $d_p < 2$ nm particles (Figure 5(b)). Similarly, the indoor atmospheric condensational particle growth rates from sVCP use activities are significantly higher than those from outdoor remote NPF events. Consequently, indoor NPF events release up to 4 orders of magnitude more indoor atmospheric NCA compared to outdoor atmospheric NCA during outdoor NPF events (Figure 5(c)). Despite having higher coagulation sinks during indoor NPF events (0.001−1 s^{-1}) compared to outdoor NPF events (0.0008−0.003 s^{-1}), the high particle nucleation rates during indoor NPF events lead to a significantly greater presence of indoor atmospheric NCA. It should be noted that outdoor nanoparticle levels are regularly monitored; however, this is not true for indoor environments. sVCPs, readily available in major retail stores, can initiate indoor atmospheric NPF at much faster rates during our everyday activities, even at lower O_3 mixing ratios. The mean O_3 mixing ratio during the NPF events in our study is 12.1 ppb, which is comparable to the observed indoor O_3 levels in residential environments (mean: 14.9 ppb)[109] and higher than those in office environments (median: 4.6 ppb).[110] Indoor O_3 mixing ratios may increase further, considering the implications of recent recommendations to enhance outdoor air exchange rates to mitigate airborne virus transmission risks, such as those associated with SARS-CoV-2.[111] However, number concentrations of indoor nanoparticles down to molecular length-scales are neither regulated nor routinely monitored.

Linking Indoor NPF Parameters to Respiratory Exposures. sVCP-initiated indoor atmospheric NPF can pose significant respiratory risks for indoor occupants. A 20 min use of an indoor sVCP can result in between 10^{11} and 10^{13} NCA being deposited in an adult human respiratory system. Such high respiratory exposure rivals or exceeds that from primary combustion sources such as propane gas stoves and heavy-duty diesel engines.[20,85] Additionally, NPF in outdoor environments has been reported to result in the inhalation of approximately 3.3×10^{10} nanoparticles (3−100 nm) per day in the adult pulmonary region.[112] In comparison, our study observed a mean respiratory tract deposited dose rate of 2.8×10^8 nanoparticles (10−50 nm) per minute in the adult pulmonary region during sVCP-initiated indoor atmospheric NPF events. Therefore, even 2 h of exposure to sVCP-initiated indoor atmospheric NPF throughout the day can exceed the nanoparticle inhalation exposure observed in the adult pulmonary region from outdoor NPF events.

Furthermore, we are also the first to link fundamental NPF parameters to respiratory deposition in different human respiratory tracts, as shown in Figure 6(b). The particle nucleation rate, $J_{1.75}$, is associated with the rate of deposition of NCA in the adult head airway region ($DF_{max} \sim 1$ nm), and the condensational growth rate for particles greater than 10 nm is linked to the rate of deposition of 10−50 nm particles in the adult human pulmonary region ($DF_{max} \sim 30$ nm). We observe a strong positive correlation between these parameters. This suggests that NPF events with higher nucleation rates would increase NCA deposition in the head airways region, and NPF events with a greater super-10 nm particle growth rate would enhance the deposition of 10−50 nm particles in the deeper pulmonary region. Such an association occurs because the nucleation process increases atmospheric NCA concentrations, which have a high deposition fraction in the head airways region, and the higher super-10 nm particle growth rates cause the

https://doi.org/10.1021/acsestair.4c00118
ACS EST Air 2024, 1, 1276−1293

freshly nucleated particles to rapidly grow, surviving the "valley of death", up to ∼20−30 nm−the size fraction where particles are efficiently deposited in the pulmonary region of the lungs when inhaled.[2] Understanding this is important because indoor sVCP use triggers both rapid nucleation and growth of particles that can cause a higher respiratory burden for both the upper respiratory tract and the deeper pulmonary region. Establishing such linkages helps to enhance the translation of the health effects of indoor NPF to a more comprehensible level. The risk is further exacerbated by the fact that people spend considerable time indoors,[113] and activities involving sVCP use are frequent. Thus, unlike outdoor NPF, which directly impacts global climate and has secondary effects on human health, indoor NPF poses direct occupant health risks.

Limitations and Future Outlook. Our comprehensive study highlights avenues for future research and acknowledges existing limitations. First, there are measurement uncertainties with the PSMPS instrument. This includes the sensitivity of the PSM to NCA composition and the production of charger ions in the soft X-ray neutralizer of the PSMPS within the NCA size fraction.[114] Additionally, the transformation of NCA upon interaction with charger ions introduces further complexities.[115−117] The exact changes that occur during this interaction remain largely unknown,[115] complicating our ability to accurately characterize the size and properties of NCA. The data-driven charger ion correction method, as applied in this analysis, is one of the approaches to correct for charger ions, potentially leading to underestimated NCA concentrations, as detailed in Patra et al.[20] Importantly, despite the uncertainties, it should be emphasized that the measurements presented in this study predominantly capture particles resulting from terpene ozonolysis, not merely artifacts from charger ions. Studies employing PSM measurements, which do not rely on particle charging to detect NCA, have consistently demonstrated nucleation events down to 1 nm originating from terpene ozonolysis, mirroring our observations.[2,118] Furthermore, studies employing DMA-based methods have successfully utilized known electrical mobility standards to classify NCA, supporting the robustness of DMAs to classify NCA.[37,119,120]

Second, while terpenes from sVCPs can be oxidized by multiple atmospheric oxidants[121] such as O_3, OH, NO_3, or Cl, our study only discussed the oxidation of terpenes initiated by O_3 based on prevalent literature[2] and limited detection of OH radicals ($<10^5$ cm^{-3}) by the laser-induced fluorescence−fluorescence assay by gas expansion (LIF-FAGE) method in the test house,[122] establishing O_3 as the primary oxidant. However, it is important to note that the ozonolysis of terpenes proceeds with the formation of OH radicals, which participate in further oxidation reactions.[2] Third, our study did not incorporate a fast GC module at the inlet of our PTR-TOF-MS, which limits our ability to distinguish fragmentation patterns of protonated VOCs within the PTR-TOF-MS drift tube.[53] Monoterpenes and monoterpenoids, our target VOCs, produce common fragment ions,[13] and due to this, the fragmentation cannot be resolved solely with the PTR-TOF-MS. Consequently, we reported terpene mixing ratios as cumulative signals from parent and common fragment ions, representing the total monoterpene and monoterpenoid mixing ratios. Additionally, without GC data, isomer distinctions for monoterpenes and monoterpenoids were not feasible; instead, calculations of the terpene composition of the sVCPs were based on the literature (Table S2). Therefore, we conducted a sensitivity analysis on our literature-based terpene ozonolysis rates, which were found to explain previously published biogenic nucleation rates within a 20% error margin (Figure S10). Our findings underscore the need for future research to resolve individual terpene compounds and their effects on indoor NPF, particularly given recent insights into the oxidative impacts of specific monoterpenoids like linalool.[8]

Furthermore, the outdoor air ventilation rates (6.3 h^{-1}) maintained in this study are higher than those typically found in most residential homes, which range from ∼0.37 to 1.6 h^{-1} in urban areas.[123] At lower outdoor air ventilation rates, the peak terpene mixing ratios in indoor environments can reach higher levels, but simultaneously, less outdoor O_3 is introduced indoors. Our results suggest that indoor atmospheric terpene ozonolysis reactions occur in an O_3-limited regime (Figure 2). Thus, even at lower O_3 mixing ratios, higher terpene mixing ratios can drive stronger sVCP-initiated nucleation. However, lower outdoor air ventilation rates also increase the coagulation rates for nanoparticles, thereby increasing their loss rates.[124] Future studies under varying outdoor air ventilation rates are needed to fully elucidate its role in sVCP-initiated indoor atmospheric NPF and associated inhalation exposures.

Additionally, there are limitations associated with estimating nucleation and growth rates. We utilized the most recent equations in the literature to model these rates.[59,70] For the nucleation rate estimation, the formation of charger ions in DMA might influence the estimation of particle nucleation rates. However, the charger ion corrections applied in this study should partially address the uncertainties related to the nucleation of charger ions in our final particle number size distributions.[20] Evidence for this is the observation of very few nucleated particles in our corrected particle number size distributions during a PCP use activity, where no significant terpene emissions occurred and no nucleation was expected (Figure S6(b)). As previously discussed, our corrections might lead to an underestimation of NCA concentrations, resulting in an underestimated nucleation rate. However, with the current understanding of the dynamics of charger ions inside the DMA, it is not feasible to numerically estimate these uncertainties.

For the growth rate estimation, we corrected the apparent growth rates for coagulation processes (both intermodal and intramodal) to estimate the particle condensational growth rates. We used the mode-fitting method to estimate the apparent growth rates, which have been reported with high uncertainties in the sub-3 nm size range.[70] This was the reason that we did not estimate the particle growth rates in the NCA size fraction but instead estimated the growth rates for particles larger than 3 nm where a prominent particle mode was distinguishable. For particles larger than 3 nm, the mode-fitting method, after corrections for coagulation processes, has been observed to yield particle condensational growth rates close to true condensational growth rates.[70]

Finally, this study does not explore the potential impacts of ammonia (NH_3), human-associated organic acids, and sulfuric acid (H_2SO_4) on sVCP-initiated NPF. Human activities within the test house likely introduced NH_3 and organic acids,[125,126] with outdoor H_2SO_4 potentially introduced via mechanical ventilation or formed in situ from the ozonolysis of monoterpenes.[127] While these components, alongside biogenic ULVOCs, could synergistically influence nucleation and particle growth, the specific mechanisms—whether synergistic or due to co-condensation—remain uncertain.[30] Our findings show that particle nucleation and growth rates from terpene ozonolysis during sVCP use align with previous biogenic nucleation studies,

https://doi.org/10.1021/acsestair.4c00118
ACS EST Air 2024, 1, 1276−1293

and we observed no nucleation or growth in events without significant terpene emissions. These results suggest that terpene emissions primarily drive indoor NPF, yet the roles of other gas-phase components cannot be entirely excluded. Future research should monitor these compounds in real-time to clarify the multicomponent nucleation and growth mechanisms during indoor sVCP use.

■ ASSOCIATED CONTENT

Supporting Information

The Supporting Information is available free of charge at https://pubs.acs.org/doi/10.1021/acsestair.4c00118.

Details of the experimental protocol and particle- and gas-phase instrumentation; summary of the sVCP use activities and time-resolved evaluation of nanoparticles and terpenes during these activities; and comparison of terpene emissions and size-integrated NCA number concentrations with previously published studies (PDF)

■ AUTHOR INFORMATION

Corresponding Author

Brandon E. Boor − *Lyles School of Civil and Construction Engineering and Ray W. Herrick Laboratories, Center for High Performance Buildings, Purdue University, West Lafayette, Indiana 47907, United States;* orcid.org/0000-0003-1011-4100; Email: bboor@purdue.edu

Authors

Satya S. Patra − *Lyles School of Civil and Construction Engineering and Ray W. Herrick Laboratories, Center for High Performance Buildings, Purdue University, West Lafayette, Indiana 47907, United States;* orcid.org/0000-0003-2099-7875

Jianghui Liu − *Lyles School of Civil and Construction Engineering, Purdue University, West Lafayette, Indiana 47907, United States*

Jinglin Jiang − *Lyles School of Civil and Construction Engineering and Ray W. Herrick Laboratories, Center for High Performance Buildings, Purdue University, West Lafayette, Indiana 47907, United States;* orcid.org/0000-0001-6271-0436

Xiaosu Ding − *Lyles School of Civil and Construction Engineering, Purdue University, West Lafayette, Indiana 47907, United States;* orcid.org/0000-0003-2730-0823

Chunxu Huang − *Lyles School of Civil and Construction Engineering and Ray W. Herrick Laboratories, Center for High Performance Buildings, Purdue University, West Lafayette, Indiana 47907, United States*

Connor Keech − *DURAG Inc., Minnetonka, Minnesota 55343, United States*

Gerhard Steiner − *GRIMM Aerosol Technik Ainring GmbH & Co. KG, Ainring 83404, Germany*

Philip S. Stevens − *Department of Chemistry and O'Neill School of Public and Environmental Affairs, Indiana University, Bloomington, Indiana 47405, United States;* orcid.org/0000-0001-9899-4215

Nusrat Jung − *Lyles School of Civil and Construction Engineering, Purdue University, West Lafayette, Indiana 47907, United States;* orcid.org/0000-0002-8874-8923

Complete contact information is available at: https://pubs.acs.org/10.1021/acsestair.4c00118

Notes

The authors declare the following competing financial interest(s): G.S. is a full-time employee of GRIMM Aerosol Technik Ainring GmbH & Co. KG, which has a potential direct or indirect financial interest in the subject matter discussed in the manuscript. C.K. is a full-time employee of DURAG Inc., which has a potential direct or indirect financial interest in the subject matter discussed in the manuscript.

■ ACKNOWLEDGMENTS

Financial support was provided by the National Science Foundation (CBET-1847493 to B.E.B.), the Alfred P. Sloan Foundation Chemistry of the Indoor Environments Program (G-2018-11061 to B.E.B. and P.S.S.), Purdue University start-up funds (to N.J.), and an American Society of Heating, Refrigerating, and Air Conditioning Engineers Graduate Student Grant-In-Aid Award (to S.S.P.).

■ REFERENCES

(1) McDonald, B. C.; de Gouw, J. A.; Gilman, J. B.; Jathar, S. H.; Akherati, A.; Cappa, C. D.; Jimenez, J. L.; Lee-Taylor, J.; Hayes, P. L.; McKeen, S. A.; Cui, Y. Y.; Kim, S.-W.; Gentner, D. R.; Isaacman-VanWertz, G.; Goldstein, A. H.; Harley, R. A.; Frost, G. J.; Roberts, J. M.; Ryerson, T. B.; Trainer, M. Volatile Chemical Products Emerging as Largest Petrochemical Source of Urban Organic Emissions. *Science* **2018**, *359* (6377), 760−764.

(2) Rosales, C. M. F.; Jiang, J.; Lahib, A.; Bottorff, B. P.; Reidy, E. K.; Kumar, V.; Tasoglou, A.; Huber, H.; Dusanter, S.; Tomas, A.; Boor, B. E.; Stevens, P. S. Chemistry and Human Exposure Implications of Secondary Organic Aerosol Production from Indoor Terpene Ozonolysis. *Sci. Adv.* **2022**, *8* (8), No. eabj9156.

(3) Sasidharan, S.; He, Y.; Akherati, A.; Li, Q.; Li, W.; Cocker, D.; McDonald, B. C.; Coggon, M. M.; Seltzer, K. M.; Pye, H. O. T.; Pierce, J. R.; Jathar, S. H. Secondary Organic Aerosol Formation from Volatile Chemical Product Emissions: Model Parameters and Contributions to Anthropogenic Aerosol. *Environ. Sci. Technol.* **2023**, *57* (32), 11891−11902.

(4) Pennington, E. A.; Seltzer, K. M.; Murphy, B. N.; Qin, M.; Seinfeld, J. H.; Pye, H. O. T. Modeling Secondary Organic Aerosol Formation from Volatile Chemical. *Atmos Chem. Phys.* **2021**, *21* (24), 18247−18261.

(5) Nazaroff, W. W.; Weschler, C. J. Cleaning Products and Air Fresheners: Exposure to Primary and Secondary Air Pollutants. *Atmos. Environ.* **2004**, *38* (18), 2841−2865.

(6) Coggon, M. M.; Gkatzelis, G. I.; McDonald, B. C.; Gilman, J. B.; Schwantes, R. H.; Abuhassan, N.; Aikin, K. C.; Arend, M. F.; Berkoff, T. A.; Brown, S. S.; Campos, T. L.; Dickerson, R. R.; Gronoff, G.; Hurley, J. F.; Isaacman-VanWertz, G.; Koss, A. R.; Li, M.; McKeen, S. A.; Moshary, F.; Peischl, J.; Pospisilova, V.; Ren, X.; Wilson, A.; Wu, Y.; Trainer, M.; Warneke, C. Volatile Chemical Product Emissions Enhance Ozone and Modulate Urban Chemistry. *Proc. Natl. Acad. Sci. U. S. A.* **2021**, *118* (32), No. e2026653118.

(7) Gkatzelis, G. I.; Coggon, M. M.; McDonald, B. C.; Peischl, J.; Aikin, K. C.; Gilman, J. B.; Trainer, M.; Warneke, C. Identifying Volatile Chemical Product Tracer Compounds in U.S. Cities. *Environ. Sci. Technol.* **2021**, *55* (1), 188−199.

(8) Fu, Z.; Guo, S.; Yu, Y.; Xie, H.-B.; Li, S.; Lv, D.; Zhou, P.; Song, K.; Chen, Z.; Tan, R.; Hu, K.; Shen, R.; Yao, M.; Hu, M. Oxidation Mechanism and Toxicity Evolution of Linalool, a Typical Indoor Volatile Chemical Product. *Environment & Health* **2024**, *2* (7), 486−498.

(9) Steinemann, A. Volatile Emissions from Common Consumer Products. *Air Qual Atmos Health* **2015**, *8* (3), 273−281.

(10) Nematollahi, N.; Kolev, S. D.; Steinemann, A. Volatile Chemical Emissions from 134 Common Consumer Products. *Air Qual Atmos Health* **2019**, *12* (11), 1259−1265.

(11) Steinemann, A. The Fragranced Products Phenomenon: Air Quality and Health, Science and Policy. *Air Qual Atmos Health* **2021**, *14* (2), 235−243.
(12) Grand View Research. *Home Fragrance Market Size, Share & Trends Report, 2030*. https://www.grandviewresearch.com/industry-analysis/home-fragrance-market (accessed 2024−08−14).
(13) Liu, J.; Jiang, J.; Ding, X.; Patra, S. S.; Cross, J. N.; Huang, C.; Kumar, V.; Price, P.; Reidy, E. K.; Tasoglou, A.; Huber, H.; Stevens, P. S.; Boor, B. E.; Jung, N. Real-Time Evaluation of Terpene Emissions and Exposures during the Use of Scented Wax Products in Residential Buildings with PTR-TOF-MS. *Build Environ* **2024**, *255*, No. 111314.
(14) Seltzer, K. M.; Pennington, E.; Rao, V.; Murphy, B. N.; Strum, M.; Isaacs, K. K.; Pye, H. O. T. Reactive Organic Carbon Emissions from Volatile Chemical Products. *Atmos Chem. Phys.* **2021**, *21* (6), 5079−5100.
(15) Jiang, J.; Ding, X.; Patra, S. S.; Cross, J. N.; Huang, C.; Kumar, V.; Price, P.; Reidy, E. K.; Tasoglou, A.; Huber, H.; Stevens, P. S.; Boor, B. E.; Jung, N. Siloxane Emissions and Exposures during the Use of Hair Care Products in Buildings. *Environ. Sci. Technol.* **2023**, *57* (48), 19999−20009.
(16) Humes, M. B.; Wang, M.; Kim, S.; Machesky, J. E.; Gentner, D. R.; Robinson, A. L.; Donahue, N. M.; Presto, A. A. Limited Secondary Organic Aerosol Production from Acyclic Oxygenated Volatile Chemical Products. *Environ. Sci. Technol.* **2022**, *56* (8), 4806−4815.
(17) Shah, R. U.; Coggon, M. M.; Gkatzelis, G. I.; McDonald, B. C.; Tasoglou, A.; Huber, H.; Gilman, J.; Warneke, C.; Robinson, A. L.; Presto, A. A. Urban Oxidation Flow Reactor Measurements Reveal Significant Secondary Organic Aerosol Contributions from Volatile Emissions of Emerging Importance. *Environ. Sci. Technol.* **2020**, *54* (2), 714−725.
(18) Kontkanen, J.; Lehtipalo, K.; Ahonen, L.; Kangasluoma, J.; Manninen, H. E.; Hakala, J.; Rose, C.; Sellegri, K.; Xiao, S.; Wang, L.; Qi, X.; Nie, W.; Ding, A.; Yu, H.; Lee, S.; Kerminen, V.-M.; Petäjä, T.; Kulmala, M. Measurements of Sub-3 nm Particles Using a Particle Size Magnifier in different Environments: From Clean Mountain Top to Polluted Megacities. *Atmos Chem. Phys.* **2017**, *17* (3), 2163−2187.
(19) Wang, M.; Kong, W.; Marten, R.; He, X.-C.; Chen, D.; Pfeifer, J.; Heitto, A.; Kontkanen, J.; Dada, L.; Kürten, A.; Yli-Juuti, T.; Manninen, H. E.; Amanatidis, S.; Amorim, A.; Baalbaki, R.; Baccarini, A.; Bell, D. M.; Bertozzi, B.; Bräkling, S.; Brilke, S.; Murillo, L. C.; Chiu, R.; Chu, B.; De Menezes, L.-P.; Duplissy, J.; Finkenzeller, H.; Carracedo, L. G.; Granzin, M.; Guida, R.; Hansel, A.; Hofbauer, V.; Krechmer, J.; Lehtipalo, K.; Lamkaddam, H.; Lampimäki, M.; Lee, C. P.; Makhmutov, V.; Marie, G.; Mathot, S.; Mauldin, R. L.; Mentler, B.; Müller, T.; Onnela, A.; Partoll, E.; Petäjä, T.; Philippov, M.; Pospisilova, V.; Ranjithkumar, A.; Rissanen, M.; Rörup, B.; Scholz, W.; Shen, J.; Simon, M.; Sipilä, M.; Steiner, G.; Stolzenburg, D.; Tham, Y. J.; Tomé, A.; Wagner, A. C.; Wang, D. S.; Wang, Y.; Weber, S. K.; Winkler, P. M.; Wlasits, P. J.; Wu, Y.; Xiao, M.; Ye, Q.; Zauner-Wieczorek, M.; Zhou, X.; Volkamer, R.; Riipinen, I.; Dommen, J.; Curtius, J.; Baltensperger, U.; Kulmala, M.; Worsnop, D. R.; Kirkby, J.; Seinfeld, J. H.; El-Haddad, I.; Flagan, R. C.; Donahue, N. M. Rapid Growth of New Atmospheric Particles by Nitric Acid and Ammonia Condensation. *Nature* **2020**, *581* (7807), 184−189.
(20) Patra, S. S.; Jiang, J.; Ding, X.; Huang, C.; Reidy, E. K.; Kumar, V.; Price, P.; Keech, C.; Steiner, G.; Stevens, P.; Jung, N.; Boor, B. E. Dynamics of Nanocluster Aerosol in the Indoor Atmosphere during Gas Cooking. *PNAS Nexus* **2024**, *3* (2), No. pgae044.
(21) Poikkimäki, M.; Koljonen, V.; Leskinen, N.; Närhi, M.; Kangasniemi, O.; Kausiala, O.; Dal Maso, M. Nanocluster Aerosol Emissions of a 3D Printer. *Environ. Sci. Technol.* **2019**, *53* (23), 13618−13628.
(22) Yang, S.; Licina, D.; Weschler, C. J.; Wang, N.; Zannoni, N.; Li, M.; Vanhanen, J.; Langer, S.; Wargocki, P.; Williams, J.; Bekö, G. Ozone Initiates Human-Derived Emission of Nanocluster Aerosols. *Environ. Sci. Technol.* **2021**, *55* (21), 14536−14545.
(23) Yang, S.; Müller, T.; Wang, N.; Bekö, G.; Zhang, M.; Merizak, M.; Wargocki, P.; Williams, J.; Licina, D. Influence of Ventilation on Formation and Growth of 1−20 nm Particles via Ozone−Human Chemistry. *Environ. Sci. Technol.* **2024**, *58* (10), 4704−4715.
(24) Garcia, G. J. M.; Schroeter, J. D.; Kimbell, J. S. Olfactory Deposition of Inhaled Nanoparticles in Humans. *Inhal Toxicol* **2015**, *27* (8), 394−403.
(25) Thomsen, D.; Iversen, E. M.; Skønager, J. T.; Luo, Y.; Li, L.; Roldin, P.; Priestley, M.; Pedersen, H. B.; Hallquist, M.; Ehn, M.; Bilde, M.; Glasius, M. The Effect of Temperature and Relative Humidity on Secondary Organic Aerosol Formation from Ozonolysis of Δ3-Carene. *Environmental Science: Atmospheres* **2024**, *4* (1), 88−103.
(26) Simon, M.; Dada, L.; Heinritzi, M.; Scholz, W.; Stolzenburg, D.; Fischer, L.; Wagner, A. C.; Kürten, A.; Rörup, B.; He, X.-C.; Almeida, J.; Baalbaki, R.; Baccarini, A.; Bauer, P. S.; Beck, L.; Bergen, A.; Bianchi, F.; Bräkling, S.; Brilke, S.; Caudillo, L.; Chen, D.; Chu, B.; Dias, A.; Draper, D. C.; Duplissy, J.; El-Haddad, I.; Finkenzeller, H.; Frege, C.; Gonzalez-Carracedo, L.; Gordon, H.; Granzin, M.; Hakala, J.; Hofbauer, V.; Hoyle, C. R.; Kim, C.; Kong, W.; Lamkaddam, H.; Lee, C. P.; Lehtipalo, K.; Leiminger, M.; Mai, H.; Manninen, H. E.; Marie, G.; Marten, R.; Mentler, B.; Molteni, U.; Nichman, L.; Nie, W.; Ojdanic, A.; Onnela, A.; Partoll, E.; Petäjä, T.; Pfeifer, J.; Philippov, M.; Quéléver, L. L. J.; Ranjithkumar, A.; Rissanen, M. P.; Schallhart, S.; Schobesberger, S.; Schuchmann, S.; Shen, J.; Sipilä, M.; Steiner, G.; Stozhkov, Y.; Tauber, C.; Tham, Y. J.; Tomé, A. R.; Vazquez-Pufleau, M.; Vogel, A. L.; Wagner, R.; Wang, M.; Wang, D. S.; Wang, Y.; Weber, S. K.; Wu, Y.; Xiao, M.; Yan, C.; Ye, P.; Ye, Q.; Zauner-Wieczorek, M.; Zhou, X.; Baltensperger, U.; Dommen, J.; Flagan, R. C.; Hansel, A.; Kulmala, M.; Volkamer, R.; Winkler, P. M.; Worsnop, D. R.; Donahue, N. M.; Kirkby, J.; Curtius, J. Molecular Understanding of New-Particle Formation from α-Pinene between −50 and + 25 °C. *Atmos Chem. Phys.* **2020**, *20* (15), 9183−9207.
(27) Stolzenburg, D.; Fischer, L.; Vogel, A. L.; Heinritzi, M.; Schervish, M.; Simon, M.; Wagner, A. C.; Dada, L.; Ahonen, L. R.; Amorim, A.; Baccarini, A.; Bauer, P. S.; Baumgartner, B.; Bergen, A.; Bianchi, F.; Breitenlechner, M.; Brilke, S.; Buenrostro Mazon, S.; Chen, D.; Dias, A.; Draper, D. C.; Duplissy, J.; El Haddad, I.; Finkenzeller, H.; Frege, C.; Fuchs, C.; Garmash, O.; Gordon, H.; He, X.; Helm, J.; Hofbauer, V.; Hoyle, C. R.; Kim, C.; Kirkby, J.; Kontkanen, J.; Kürten, A.; Lampilahti, J.; Lawler, M.; Lehtipalo, K.; Leiminger, M.; Mai, H.; Mathot, S.; Mentler, B.; Molteni, U.; Nie, W.; Nieminen, T.; Nowak, J. B.; Ojdanic, A.; Onnela, A.; Passananti, M.; Petäjä, T.; Quéléver, L. L. J.; Rissanen, M. P.; Sarnela, N.; Schallhart, S.; Tauber, C.; Tomé, A.; Wagner, R.; Wang, M.; Weitz, L.; Wimmer, D.; Xiao, M.; Yan, C.; Ye, P.; Zha, Q.; Baltensperger, U.; Curtius, J.; Dommen, J.; Flagan, R. C.; Kulmala, M.; Smith, J. N.; Worsnop, D. R.; Hansel, A.; Donahue, N. M.; Winkler, P. M. Rapid Growth of Organic Aerosol Nanoparticles over a Wide Tropospheric Temperature Range. *Proc. Natl. Acad. Sci. U. S. A.* **2018**, *115* (37), 9122−9127.
(28) Kirkby, J.; Duplissy, J.; Sengupta, K.; Frege, C.; Gordon, H.; Williamson, C.; Heinritzi, M.; Simon, M.; Yan, C.; Almeida, J.; Tröstl, J.; Nieminen, T.; Ortega, I. K.; Wagner, R.; Adamov, A.; Amorim, A.; Bernhammer, A.-K.; Bianchi, F.; Breitenlechner, M.; Brilke, S.; Chen, X.; Craven, J.; Dias, A.; Ehrhart, S.; Flagan, R. C.; Franchin, A.; Fuchs, C.; Guida, R.; Hakala, J.; Hoyle, C. R.; Jokinen, T.; Junninen, H.; Kangasluoma, J.; Kim, J.; Krapf, M.; Kürten, A.; Laaksonen, A.; Lehtipalo, K.; Makhmutov, V.; Mathot, S.; Molteni, U.; Onnela, A.; Peräkylä, O.; Piel, F.; Petäjä, T.; Praplan, A. P.; Pringle, K.; Rap, A.; Richards, N. A. D.; Riipinen, I.; Rissanen, M. P.; Rondo, L.; Sarnela, N.; Schobesberger, S.; Scott, C. E.; Seinfeld, J. H.; Sipilä, M.; Steiner, G.; Stozhkov, Y.; Stratmann, F.; Tomé, A.; Virtanen, A.; Vogel, A. L.; Wagner, A. C.; Wagner, P. E.; Weingartner, E.; Wimmer, D.; Winkler, P. M.; Ye, P.; Zhang, X.; Hansel, A.; Dommen, J.; Donahue, N. M.; Worsnop, D. R.; Baltensperger, U.; Kulmala, M.; Carslaw, K. S.; Curtius, J. Ion-Induced Nucleation of Pure Biogenic Particles. *Nature* **2016**, *533* (7604), 521−526.
(29) Li, X.; Chee, S.; Hao, J.; Abbatt, J. P. D.; Jiang, J.; Smith, J. N. Relative Humidity Effect on the Formation of Highly Oxidized Molecules and new Particles during Monoterpene Oxidation. *Atmos Chem. Phys.* **2019**, *19* (3), 1555−1570.

(30) Kirkby, J.; Amorim, A.; Baltensperger, U.; Carslaw, K. S.; Christoudias, T.; Curtius, J.; Donahue, N. M.; Haddad, I. El; Flagan, R. C.; Gordon, H.; Hansel, A.; Harder, H.; Junninen, H.; Kulmala, M.; Kürten, A.; Laaksonen, A.; Lehtipalo, K.; Lelieveld, J.; Möhler, O.; Riipinen, I.; Stratmann, F.; Tomé, A.; Virtanen, A.; Volkamer, R.; Winkler, P. M.; Worsnop, D. R. Atmospheric New Particle Formation from the CERN CLOUD Experiment. *Nat. Geosci* **2023**, *16* (11), 948−957.

(31) Caudillo, L.; Rörup, B.; Heinritzi, M.; Marie, G.; Simon, M.; Wagner, A. C.; Müller, T.; Granzin, M.; Amorim, A.; Ataei, F.; Baalbaki, R.; Bertozzi, B.; Brasseur, Z.; Chiu, R.; Chu, B.; Dada, L.; Duplissy, J.; Finkenzeller, H.; Gonzalez Carracedo, L.; He, X.-C.; Hofbauer, V.; Kong, W.; Lamkaddam, H.; Lee, C. P.; Lopez, B.; Mahfouz, N. G. A.; Makhmutov, V.; Manninen, H. E.; Marten, R.; Massabò, D.; Mauldin, R. L.; Mentler, B.; Molteni, U.; Onnela, A.; Pfeifer, J.; Philippov, M.; Piedehierro, A. A.; Schervish, M.; Scholz, W.; Schulze, B.; Shen, J.; Stolzenburg, D.; Stozhkov, Y.; Surdu, M.; Tauber, C.; Tham, Y. J.; Tian, P.; Tomé, A.; Vogt, S.; Wang, M.; Wang, D. S.; Weber, S. K.; Welti, A.; Yonghong, W.; Yusheng, W.; Zauner-Wieczorek, M.; Baltensperger, U.; El Haddad, I.; Flagan, R. C.; Hansel, A.; Höhler, K.; Kirkby, J.; Kulmala, M.; Lehtipalo, K.; Möhler, O.; Saathoff, H.; Volkamer, R.; Winkler, P. M.; Donahue, N. M.; Kürten, A.; Curtius, J. Chemical Composition of Nanoparticles from α-Pinene Nucleation and the Influence of Isoprene and Relative Humidity at Low Temperature. *Atmos Chem. Phys.* **2021**, *21* (22), 17099−17114.

(32) Heinritzi, M.; Dada, L.; Simon, M.; Stolzenburg, D.; Wagner, A. C.; Fischer, L.; Ahonen, L. R.; Amanatidis, S.; Baalbaki, R.; Baccarini, A.; Bauer, P. S.; Baumgartner, B.; Bianchi, F.; Brilke, S.; Chen, D.; Chiu, R.; Dias, A.; Dommen, J.; Duplissy, J.; Finkenzeller, H.; Frege, C.; Fuchs, C.; Garmash, O.; Gordon, H.; Granzin, M.; El Haddad, I.; He, X.; Helm, J.; Hofbauer, V.; Hoyle, C. R.; Kangasluoma, J.; Keber, T.; Kim, C.; Kürten, A.; Lamkaddam, H.; Laurila, T. M.; Lampilahti, J.; Lee, C. P.; Lehtipalo, K.; Leiminger, M.; Mai, H.; Makhmutov, V.; Manninen, H. E.; Marten, R.; Mathot, S.; Mauldin, R. L.; Mentler, B.; Molteni, U.; Müller, T.; Nie, W.; Nieminen, T.; Onnela, A.; Partoll, E.; Passananti, M.; Petäjä, T.; Pfeifer, J.; Pospisilova, V.; Quéléver, L. L. J.; Rissanen, M. P.; Rose, C.; Schobesberger, S.; Scholz, W.; Scholze, K.; Sipilä, M.; Steiner, G.; Stozhkov, Y.; Tauber, C.; Tham, Y. J.; Vazquez-Pufleau, M.; Virtanen, A.; Vogel, A. L.; Volkamer, R.; Wagner, R.; Wang, M.; Weitz, L.; Wimmer, D.; Xiao, M.; Yan, C.; Ye, P.; Zha, Q.; Zhou, X.; Amorim, A.; Baltensperger, U.; Hansel, A.; Kulmala, M.; Tomé, A.; Winkler, P. M.; Worsnop, D. R.; Donahue, N. M.; Kirkby, J.; Curtius, J. Molecular Understanding of the Suppression of New-Particle Formation by Isoprene. *Atmos Chem. Phys.* **2020**, *20* (20), 11809−11821.

(33) Ye, Q.; Wang, M.; Hofbauer, V.; Stolzenburg, D.; Chen, D.; Schervish, M.; Vogel, A.; Mauldin, R. L.; Baalbaki, R.; Brilke, S.; Dada, L.; Dias, A.; Duplissy, J.; El Haddad, I.; Finkenzeller, H.; Fischer, L.; He, X.; Kim, C.; Kürten, A.; Lamkaddam, H.; Lee, C. P.; Lehtipalo, K.; Leiminger, M.; Manninen, H. E.; Marten, R.; Mentler, B.; Partoll, E.; Petäjä, T.; Rissanen, M.; Schobesberger, S.; Schuchmann, S.; Simon, M.; Tham, Y. J.; Vazquez-Pufleau, M.; Wagner, A. C.; Wang, Y.; Wu, Y.; Xiao, M.; Baltensperger, U.; Curtius, J.; Flagan, R.; Kirkby, J.; Kulmala, M.; Volkamer, R.; Winkler, P. M.; Worsnop, D.; Donahue, N. M. Molecular Composition and Volatility of Nucleated Particles from α-Pinene Oxidation between − 50 °C and + 25 °C. *Environ. Sci. Technol.* **2019**, *53* (21), 12357−12365.

(34) Zhao, J.; Häkkinen, E.; Graeffe, F.; Krechmer, J. E.; Canagaratna, M. R.; Worsnop, D. R.; Kangasluoma, J.; Ehn, M. A Combined Gas- and Particle-Phase Analysis of Highly Oxygenated Organic Molecules (HOMs) from α-Pinene Ozonolysis. *Atmos Chem. Phys.* **2023**, *23* (6), 3707−3730.

(35) Jeong, S.-G.; Wallace, L.; Rim, D. Contributions of Coagulation, Deposition, and Ventilation to the Removal of Airborne Nanoparticles in Indoor Environments. *Environ. Sci. Technol.* **2021**, *55* (14), 9730−9739.

(36) Kangasluoma, J.; Kontkanen, J. On the Sources of Uncertainty in the Sub-3 nm Particle Concentration Measurement. *J. Aerosol Sci.* **2017**, *112*, 34−51.

(37) Stolzenburg, D.; Steiner, G.; Winkler, P. M. A DMA-Train for Precision Measurement of Sub-10 nm Aerosol Dynamics. *Atmos Meas Tech* **2017**, *10* (4), 1639−1651.

(38) Ding, X.; Lu, H.; Jiang, J.; Tasoglou, A.; Shah, A. D.; Jung, N. Real-Time Indoor Sensing of Volatile Organic Compounds during Building Disinfection Events via Photoionization Detection and Proton Transfer Reaction Mass Spectrometry. *Build Environ* **2023**, *246*, No. 110953.

(39) Ding, X.; Jiang, J.; Tasoglou, A.; Huber, H.; Shah, A. D.; Jung, N. Evaluation of Workplace Exposures to Volatile Chemicals During COVID-19 Building Disinfection Activities with Proton Transfer Reaction Mass Spectrometry. *Ann. Work Expo Health* **2023**, *67* (4), 546−551.

(40) Jiang, J.; Ding, X.; Isaacson, K. P.; Tasoglou, A.; Huber, H.; Shah, A. D.; Jung, N.; Boor, B. E. Ethanol-Based Disinfectant Sprays Drive Rapid Changes in the Chemical Composition of Indoor Air in Residential Buildings. *J. Hazard. Mater. Letters* **2021**, *2*, No. 100042.

(41) Jiang, J.; Ding, X.; Tasoglou, A.; Huber, H.; Shah, A. D.; Jung, N.; Boor, B. E. Real-Time Measurements of Botanical Disinfectant Emissions, Transformations, and Multiphase Inhalation Exposures in Buildings. *Environ. Sci. Technol. Lett.* **2021**, *8* (7), 558−566.

(42) Pagonis, D.; Algrim, L. B.; Price, D. J.; Day, D. A.; Handschy, A. V.; Stark, H.; Miller, S. L.; de Gouw, J. A.; Jimenez, J. L.; Ziemann, P. J. Autoxidation of Limonene Emitted in a University Art Museum. *Environ. Sci. Technol. Lett.* **2019**, *6* (9), 520−524.

(43) Vartiainen, E.; Kulmala, M.; Ruuskanen, T. M.; Taipale, R.; Rinne, J.; Vehkamäki, H. Formation and Growth of Indoor Air Aerosol Particles as a Result of D-Limonene Oxidation. *Atmos. Environ.* **2006**, *40* (40), 7882−7892.

(44) Jiang, J.; Jung, N.; Boor, B. E. Using Building Energy and Smart Thermostat Data to Evaluate Indoor Ultrafine Particle Source and Loss Processes in a Net-Zero Energy House. *ACS ES&T Engineering* **2021**, *1* (4), 780−793.

(45) Patra, S. S.; Ramsisaria, R.; Du, R.; Wu, T.; Boor, B. E. A Machine Learning Field Calibration Method for Improving the Performance of Low-Cost Particle Sensors. *Build Environ* **2021**, *190*, No. 107457.

(46) Yamada, M.; Takaya, M.; Ogura, I. Performance Evaluation of Newly Developed Portable Aerosol Sizers Used for Nanomaterial Aerosol Measurements. *Ind. Health* **2015**, *53* (6), 511−516.

(47) Vo, E.; Horvatin, M.; Zhuang, Z. Performance Comparison of Field Portable Instruments to the Scanning Mobility Particle Sizer Using Monodispersed and Polydispersed Sodium Chloride Aerosols. *Ann. Work Expo Health* **2018**, *62* (6), 711−720.

(48) Fonseca, A. S.; Viana, M.; Pérez, N.; Alastuey, A.; Querol, X.; Kaminski, H.; Todea, A. M.; Monz, C.; Asbach, C. Intercomparison of a Portable and Two Stationary Mobility Particle Sizers for Nanoscale Aerosol Measurements. *Aerosol Sci. Technol.* **2016**, *50* (7), 653−668.

(49) Hsiao, T.-C.; Lee, Y.-C.; Chen, K.-C.; Ye, W.-C.; Sopajaree, K.; Tsai, Y. I. Experimental Comparison of Two Portable and Real-Time Size Distribution Analyzers for Nano/Submicron Aerosol Measurements. *Aerosol Air Qual Res.* **2016**, *16* (4), 919−929.

(50) Wolberg, G.; Alfy, I. Monotonic Cubic Spline Interpolation. In *1999 Proceedings Computer Graphics International*; IEEE, 1999.

(51) Lindinger, W.; Hansel, A.; Jordan, A. On-Line Monitoring of Volatile Organic Compounds at pptv Levels by Means of Proton-Transfer-Reaction Mass Spectrometry (PTR-MS) Medical Applications, Food Control and Environmental Research. *Int. J. Mass Spectrom Ion Process* **1998**, *173* (3), 191−241.

(52) Blake, R. S.; Monks, P. S.; Ellis, A. M. Proton-Transfer Reaction Mass Spectrometry. *Chem. Rev.* **2009**, *109* (3), 861−896.

(53) Claflin, M. S.; Pagonis, D.; Finewax, Z.; Handschy, A. V.; Day, D. A.; Brown, W. L.; Jayne, J. T.; Worsnop, D. R.; Jimenez, J. L.; Ziemann, P. J.; de Gouw, J.; Lerner, B. M. An in Situ Gas Chromatograph with Automatic Detector Switching between PTR- and EI-TOF-MS: Isomer-Resolved Measurements of Indoor Air. *Atmos Meas Tech* **2021**, *14* (1), 133−152.

(54) Xiong, F.; McAvey, K. M.; Pratt, K. A.; Groff, C. J.; Hostetler, M. A.; Lipton, M. A.; Starn, T. K.; Seeley, J. V.; Bertman, S. B.; Teng, A. P.; Crounse, J. D.; Nguyen, T. B.; Wennberg, P. O.; Misztal, P. K.;

https://doi.org/10.1021/acsestair.4c00118
ACS EST Air 2024, 1, 1276−1293

Goldstein, A. H.; Guenther, A. B.; Koss, A. R.; Olson, K. F.; de Gouw, J. A.; Baumann, K.; Edgerton, E. S.; Feiner, P. A.; Zhang, L.; Miller, D. O.; Brune, W. H.; Shepson, P. B. Observation of Isoprene Hydroxynitrates in the Southeastern United States and Implications for the Fate of NO_x. *Atmos Chem. Phys.* **2015**, *15* (19), 11257−11272.
(55) Bsaibes, S.; Al Ajami, M.; Mermet, K.; Truong, F.; Batut, S.; Hecquet, C.; Dusanter, S.; Léornadis, T.; Sauvage, S.; Kammer, J.; Flaud, P.-M.; Perraudin, E.; Villenave, E.; Locoge, N.; Gros, V.; Schoemaecker, C. Variability of Hydroxyl Radical (OH) Reactivity in the Landes Maritime Pine Forest: Results from the LANDEX Campaign 2017. *Atmos Chem. Phys.* **2020**, *20* (3), 1277−1300.
(56) Kulmala, M.; Petäjä, T.; Nieminen, T.; Sipilä, M.; Manninen, H. E.; Lehtipalo, K.; Dal Maso, M.; Aalto, P. P.; Junninen, H.; Paasonen, P.; Riipinen, I.; Lehtinen, K. E. J.; Laaksonen, A.; Kerminen, V.-M. Measurement of the Nucleation of Atmospheric Aerosol Particles. *Nat. Protoc* **2012**, *7* (9), 1651−1667.
(57) Sulo, J.; Sarnela, N.; Kontkanen, J.; Ahonen, L.; Paasonen, P.; Laurila, T.; Jokinen, T.; Kangasluoma, J.; Junninen, H.; Sipilä, M.; Petäjä, T.; Kulmala, M.; Lehtipalo, K. Long-Term Measurement of Sub-3 nm Particles and Their Precursor Gases in the Boreal Forest. *Atmos Chem. Phys.* **2021**, *21* (2), 695−715.
(58) Ehn, M.; Thornton, J. A.; Kleist, E.; Sipilä, M.; Junninen, H.; Pullinen, I.; Springer, M.; Rubach, F.; Tillmann, R.; Lee, B.; Lopez-Hilfiker, F.; Andres, S.; Acir, I.-H.; Rissanen, M.; Jokinen, T.; Schobesberger, S.; Kangasluoma, J.; Kontkanen, J.; Nieminen, T.; Kurtén, T.; Nielsen, L. B.; Jørgensen, S.; Kjaergaard, H. G.; Canagaratna, M.; Maso, M. D.; Berndt, T.; Petäjä, T.; Wahner, A.; Kerminen, V.-M.; Kulmala, M.; Worsnop, D. R.; Wildt, J.; Mentel, T. F. A Large Source of Low-Volatility Secondary Organic Aerosol. *Nature* **2014**, *506* (7489), 476−479.
(59) Cai, R.; Jiang, J. A New Balance Formula to Estimate New Particle Formation Rate: Reevaluating Effect of Coagulation Scavenging. *Atmos Chem. Phys.* **2017**, *17* (20), 12659−12675.
(60) Kirkby, J.; Curtius, J.; Almeida, J.; Dunne, E.; Duplissy, J.; Ehrhart, S.; Franchin, A.; Gagné, S.; Ickes, L.; Kürten, A.; Kupc, A.; Metzger, A.; Riccobono, F.; Rondo, L.; Schobesberger, S.; Tsagkogeorgas, G.; Wimmer, D.; Amorim, A.; Bianchi, F.; Breitenlechner, M.; David, A.; Dommen, J.; Downard, A.; Ehn, M.; Flagan, R. C.; Haider, S.; Hansel, A.; Hauser, D.; Jud, W.; Junninen, H.; Kreissl, F.; Kvashin, A.; Laaksonen, A.; Lehtipalo, K.; Lima, J.; Lovejoy, E. R.; Makhmutov, V.; Mathot, S.; Mikkilä, J.; Minginette, P.; Mogo, S.; Nieminen, T.; Onnela, A.; Pereira, P.; Petäjä, T.; Schnitzhofer, R.; Seinfeld, J. H.; Sipilä, M.; Stozhkov, Y.; Stratmann, F.; Tomé, A.; Vanhanen, J.; Viisanen, Y.; Vrtala, A.; Wagner, P. E.; Walther, H.; Weingartner, E.; Wex, H.; Winkler, P. M.; Carslaw, K. S.; Worsnop, D. R.; Baltensperger, U.; Kulmala, M. Role of Sulphuric Acid, Ammonia and Galactic Cosmic Rays in Atmospheric Aerosol Nucleation. *Nature* **2011**, *476* (7361), 429−433.
(61) Kulmala, M.; Vehkamäki, H.; Petäjä, T.; Dal Maso, M.; Lauri, A.; Kerminen, V.-M.; Birmili, W.; McMurry, P. H. Formation and Growth Rates of Ultrafine Atmospheric Particles: A Review of Observations. *J. Aerosol Sci.* **2004**, *35* (2), 143−176.
(62) Lai, A. C. K.; Nazaroff, W. W. Modeling Indoor Particle Deposition from Turbulent Flow onto Smooth Surfaces. *J. Aerosol. Sci.* **2000**, *31* (4), 463−476.
(63) Tuovinen, S.; Cai, R.; Kerminen, V.-M.; Jiang, J.; Yan, C.; Kulmala, M.; Kontkanen, J. Survival Probabilities of Atmospheric Particles: Comparison Based on Theory, Cluster Population Simulations, and Observations in Beijing. *Atmos Chem. Phys.* **2022**, *22* (22), 15071−15091.
(64) Rim, D.; Choi, J.-I.; Wallace, L. A. Size-Resolved Source Emission Rates of Indoor Ultrafine Particles Considering Coagulation. *Environ. Sci. Technol.* **2016**, *50* (18), 10031−10038.
(65) Cai, R.; Häkkinen, E.; Yan, C.; Jiang, J.; Kulmala, M.; Kangasluoma, J. The Effectiveness of the Coagulation Sink of 3−10 nm Atmospheric Particles. *Atmos Chem. Phys.* **2022**, *22* (17), 11529−11541.
(66) Cai, R.; Li, C.; He, X.-C.; Deng, C.; Lu, Y.; Yin, R.; Yan, C.; Wang, L.; Jiang, J.; Kulmala, M.; Kangasluoma, J. Impacts of Coagulation on the Appearance Time Method for New Particle Growth Evaluation and Their Corrections. *Atmos Chem. Phys.* **2021**, *21* (3), 2287−2304.
(67) Dal Maso, M.; Kulmala, M.; Lehtinen, K. E. J.; Mäkelä, J. M.; Aalto, P.; O'Dowd, C. D. Condensation and Coagulation Sinks and Formation of Nucleation Mode Particles in Coastal and Boreal Forest Boundary Layers. *J. Geophys. Res.: Atmos.* **2002**, *107* (D19), PAR2−1−PAR 2−10.
(68) Hussein, T.; Martikainen, J.; Junninen, H.; Sogacheva, L.; Wagner, R.; Maso, M. D.; Riipinen, I.; Aalto, P. P.; Kulmala, M. Observation of Regional New Particle Formation in the Urban Atmosphere. *Tellus B: Chem. Phys. Meteorol.* **2008**, *60* (4), 509−521.
(69) Leppä, J.; Anttila, T.; Kerminen, V.-M.; Kulmala, M.; Lehtinen, K. E. J. Atmospheric New Particle Formation: Real and Apparent Growth of Neutral and Charged Particles. *Atmos Chem. Phys.* **2011**, *11* (10), 4939−4955.
(70) Stolzenburg, D.; Cai, R.; Blichner, S. M.; Kontkanen, J.; Zhou, P.; Makkonen, R.; Kerminen, V.-M.; Kulmala, M.; Riipinen, I.; Kangasluoma, J. Atmospheric Nanoparticle Growth. *Rev. Mod. Phys.* **2023**, *95* (4), No. 45002.
(71) Wu, T.; Täubel, M.; Holopainen, R.; Viitanen, A.-K.; Vainiotalo, S.; Tuomi, T.; Keskinen, J.; Hyvärinen, A.; Hämeri, K.; Saari, S. E.; Boor, B. E. Infant and Adult Inhalation Exposure to Resuspended Biological Particulate Matter. *Environ. Sci. Technol.* **2018**, *52* (1), 237−247.
(72) Morawska, L.; He, C.; Johnson, G.; Guo, H.; Uhde, E.; Ayoko, G. Ultrafine Particles in Indoor Air of a School: Possible Role of Secondary Organic Aerosols. *Environ. Sci. Technol.* **2009**, *43* (24), 9103−9109.
(73) Li, H.; Canagaratna, M. R.; Riva, M.; Rantala, P.; Zhang, Y.; Thomas, S.; Heikkinen, L.; Flaud, P.-M.; Villenave, E.; Perraudin, E.; Worsnop, D.; Kulmala, M.; Ehn, M.; Bianchi, F. Atmospheric Organic Vapors in Two European Pine Forests Measured by a Vocus PTR-TOF: Insights into Monoterpene and Sesquiterpene Oxidation Processes. *Atmos Chem. Phys.* **2021**, *21* (5), 4123−4147.
(74) Farmer, D. K.; Vance, M. E.; Abbatt, J. P. D.; Abeleira, A.; Alves, M. R.; Arata, C.; Boedicker, E.; Bourne, S.; Cardoso-Saldaña, F.; Corsi, R.; DeCarlo, P. F.; Goldstein, A. H.; Grassian, V. H.; Hildebrandt Ruiz, L.; Jimenez, J. L.; Kahan, T. F.; Katz, E. F.; Mattila, J. M.; Nazaroff, W. W.; Novoselac, A.; O'Brien, R. E.; Or, V. W.; Patel, S.; Sankhyan, S.; Stevens, P. S.; Tian, Y.; Wade, M.; Wang, C.; Zhou, S.; Zhou, Y. Overview of HOMEChem: House Observations of Microbial and Environmental Chemistry. *Environ. Sci.: Processes Impacts* **2019**, *21* (8), 1280−1300.
(75) Bouzidi, H.; Fayad, L.; Coeur, C.; Houzel, N.; Petitprez, D.; Faccinetto, A.; Wu, J.; Tomas, A.; Ondráček, J.; Schwarz, J.; Ždímal, V.; Zuend, A. Hygroscopic Growth and CCN Activity of Secondary Organic Aerosol Produced from Dark Ozonolysis of γ-Terpinene. *Sci. Total Environ.* **2022**, *817*, No. 153010.
(76) Chen, J.; Griffin, R. J. Modeling Secondary Organic Aerosol Formation from Oxidation of α-Pinene, β-Pinene, and d-Limonene. *Atmos. Environ.* **2005**, *39* (40), 7731−7744.
(77) Gong, Y.; Chen, Z.; Li, H. The Oxidation Regime and SOA Composition in Limonene Ozonolysis: Roles of different Double Bonds, Radicals, and Water. *Atmos Chem. Phys.* **2018**, *18* (20), 15105−15123.
(78) Waring, M. S. Secondary Organic Aerosol Formation by Limonene Ozonolysis: Parameterizing Multi-Generational Chemistry in Ozone- and Residence Time-Limited Indoor Environments. *Atmos. Environ.* **2016**, *144*, 79−86.
(79) Zhang, J.; Huff Hartz, K. E.; Pandis, S. N.; Donahue, N. M. Secondary Organic Aerosol Formation from Limonene Ozonolysis: Homogeneous and Heterogeneous Influences as a Function of NO_x. *J. Phys. Chem. A* **2006**, *110* (38), 11053−11063.
(80) Crounse, J. D.; Nielsen, L. B.; Jørgensen, S.; Kjaergaard, H. G.; Wennberg, P. O. Autoxidation of Organic Compounds in the Atmosphere. *J. Phys. Chem. Lett.* **2013**, *4* (20), 3513−3520.
(81) Benoit, R.; Belhadj, N.; Dbouk, Z.; Lailliau, M.; Dagaut, P. On the Formation of Highly Oxidized Pollutants by Autoxidation of Terpenes under Low-Temperature-Combustion Conditions: The Case of

https://doi.org/10.1021/acsestair.4c00118
ACS EST Air 2024, 1, 1276−1293

Limonene and α-Pinene. *Atmos Chem. Phys.* **2023**, *23* (10), 5715−5733.
(82) Berndt, T.; Mentler, B.; Scholz, W.; Fischer, L.; Herrmann, H.; Kulmala, M.; Hansel, A. Accretion Product Formation from Ozonolysis and OH Radical Reaction of α-Pinene: Mechanistic Insight and the Influence of Isoprene and Ethylene. *Environ. Sci. Technol.* **2018**, *52* (19), 11069−11077.
(83) Waring, M. S.; Wells, J. R.; Siegel, J. A. Secondary Organic Aerosol Formation from Ozone Reactions with Single Terpenoids and Terpenoid Mixtures. *Atmos. Environ.* **2011**, *45* (25), 4235−4242.
(84) Amouei Torkmahalleh, M.; Turganova, K.; Zhigulina, Z.; Madiyarova, T.; Adotey, E. K.; Malekipirbazari, M.; Buonanno, G.; Stabile, L. Formation of Cluster Mode Particles (1−3 nm) in Preschools. *Sci. Total Environ.* **2022**, *818*, No. 151756.
(85) Rönkkö, T.; Kuuluvainen, H.; Karjalainen, P.; Keskinen, J.; Hillamo, R.; Niemi, J. V.; Pirjola, L.; Timonen, H. J.; Saarikoski, S.; Saukko, E.; Järvinen, A.; Silvennoinen, H.; Rostedt, A.; Olin, M.; Yli-Ojanperä, J.; Nousiainen, P.; Kousa, A.; Dal Maso, M. Traffic Is a Major Source of Atmospheric Nanocluster Aerosol. *Proc. Natl. Acad. Sci. U. S. A.* **2017**, *114* (29), 7549−7554.
(86) Jathar, S. H.; Sharma, N.; Bilsback, K. R.; Pierce, J. R.; Vanhanen, J.; Gordon, T. D.; Volckens, J. Emissions and Radiative Impacts of Sub-10 nm Particles from Biofuel and Fossil Fuel Cookstoves. *Aerosol Sci. Technol.* **2020**, *54* (10), 1231−1243.
(87) Yang, S.; Licina, D. Nanocluster Aerosol Formation via Ozone Chemistry on Worn Clothing: Influence of Environmental Parameters. *Build Environ* **2024**, *256*, No. 111474.
(88) O'Dowd, C. D.; Hämeri, K.; Mäkelä, J.; Väkeva, M.; Aalto, P.; de Leeuw, G.; Kunz, G. J.; Becker, E.; Hansson, H.-C.; Allen, A. G.; Harrison, R. M.; Berresheim, H.; Kleefeld, C.; Geever, M.; Jennings, S. G.; Kulmala, M. Coastal New Particle Formation: Environmental Conditions and Aerosol Physicochemical Characteristics during Nucleation Bursts. *J. Geophys. Res.: Atmos.* **2002**, *107* (D19), PAR 12−1−PAR 12−17.
(89) Suni, T.; Kulmala, M.; Hirsikko, A.; Bergman, T.; Laakso, L.; Aalto, P. P.; Leuning, R.; Cleugh, H.; Zegelin, S.; Hughes, D.; van Gorsel, E.; Kitchen, M.; Vana, M.; Horrak, U.; Mirme, S.; Mirme, A.; Sevanto, S.; Twining, J.; Tadros, C. Formation and Characteristics of Ions and Charged Aerosol Particles in a Native Australian Eucalypt Forest. *Atmos. Chem. Phys.* **2008**, *8* (1), 129−139.
(90) Kulmala, M.; Kontkanen, J.; Junninen, H.; Lehtipalo, K.; Manninen, H. E.; Nieminen, T.; Petäjä, T.; Sipilä, M.; Schobesberger, S.; Rantala, P.; Franchin, A.; Jokinen, T.; Järvinen, E.; Äijälä, M.; Kangasluoma, J.; Hakala, J.; Aalto, P. P.; Paasonen, P.; Mikkilä, J.; Vanhanen, J.; Aalto, J.; Hakola, H.; Makkonen, U.; Ruuskanen, T.; Mauldin, R. L.; Duplissy, J.; Vehkamäki, H.; Bäck, J.; Kortelainen, A.; Riipinen, I.; Kurtén, T.; Johnston, M. V.; Smith, J. N.; Ehn, M.; Mentel, T. F.; Lehtinen, K. E. J.; Laaksonen, A.; Kerminen, V.-M.; Worsnop, D. R. Direct Observations of Atmospheric Aerosol Nucleation. *Science* **2013**, *339* (6122), 943−946.
(91) Nieminen, T.; Kerminen, V.-M.; Petäjä, T.; Aalto, P. P.; Arshinov, M.; Asmi, E.; Baltensperger, U.; Beddows, D. C. S.; Beukes, J. P.; Collins, D.; Ding, A.; Harrison, R. M.; Henzing, B.; Hooda, R.; Hu, M.; Horrak, U.; Kivekäs, N.; Komsaare, K.; Krejci, R.; Kristensson, A.; Laakso, L.; Laaksonen, A.; Leaitch, W. R.; Lihavainen, H.; Mihalopoulos, N.; Németh, Z.; Nie, W.; O'Dowd, C.; Salma, I.; Sellegri, K.; Svenningsson, B.; Swietlicki, E.; Tunved, P.; Ulevicius, V.; Vakkari, V.; Vana, M.; Wiedensohler, A.; Wu, Z.; Virtanen, A.; Kulmala, M. Global Analysis of Continental Boundary Layer New Particle Formation Based on Long-Term Measurements. *Atmos. Chem. Phys.* **2018**, *18* (19), 14737−14756.
(92) Bianchi, F.; Tröstl, J.; Junninen, H.; Frege, C.; Henne, S.; Hoyle, C. R.; Molteni, U.; Herrmann, E.; Adamov, A.; Bukowiecki, N.; Chen, X.; Duplissy, J.; Gysel, M.; Hutterli, M.; Kangasluoma, J.; Kontkanen, J.; Kürten, A.; Manninen, H. E.; Münch, S.; Peräkylä, O.; Petäjä, T.; Rondo, L.; Williamson, C.; Weingartner, E.; Curtius, J.; Worsnop, D. R.; Kulmala, M.; Dommen, J.; Baltensperger, U. New Particle Formation in the Free Troposphere: A Question of Chemistry and Timing. *Science* **2016**, *352* (6289), 1109−1112.
(93) Deng, C.; Fu, Y.; Dada, L.; Yan, C.; Cai, R.; Yang, D.; Zhou, Y.; Yin, R.; Lu, Y.; Li, X.; Qiao, X.; Fan, X.; Nie, W.; Kontkanen, J.; Kangasluoma, J.; Chu, B.; Ding, A.; Kerminen, V.-M.; Paasonen, P.; Worsnop, D. R.; Bianchi, F.; Liu, Y.; Zheng, J.; Wang, L.; Kulmala, M.; Jiang, J. Seasonal Characteristics of New Particle Formation and Growth in Urban Beijing. *Environ. Sci. Technol.* **2020**, *54* (14), 8547−8557.
(94) Rose, C.; Sellegri, K.; Velarde, F.; Moreno, I.; Ramonet, M.; Weinhold, K.; Krejci, R.; Ginot, P.; Andrade, M.; Wiedensohler, A.; Laj, P. Frequent Nucleation Events at the High Altitude Station of Chacaltaya (5240 m a.s.l.), Bolivia. *Atmos. Environ.* **2015**, *102*, 18−29.
(95) Kuang, C.; Chen, M.; Zhao, J.; Smith, J.; McMurry, P. H.; Wang, J. Size and Time-Resolved Growth Rate Measurements of 1 to 5 nm Freshly Formed Atmospheric Nuclei. *Atmos Chem. Phys.* **2012**, *12* (7), 3573−3589.
(96) Su, P.; Joutsensaari, J.; Dada, L.; Zaidan, M. A.; Nieminen, T.; Li, X.; Wu, Y.; Decesari, S.; Tarkoma, S.; Petäjä, T.; Kulmala, M.; Pellikka, P. New Particle Formation Event Detection with Mask R-CNN. *Atmos Chem. Phys.* **2022**, *22* (2), 1293−1309.
(97) Sebastian, M.; Kanawade, V. P.; Soni, V. K.; Asmi, E.; Westervelt, D. M.; Vakkari, V.; Hyvärinen, A.-P.; Pierce, J. R.; Hooda, R. K. New Particle Formation and Growth to Climate-Relevant Aerosols at a Background Remote Site in the Western Himalaya. *J. Geophys. Res.: Atmos.* **2021**, *126* (7), No. e2020JD033267.
(98) Kulmala, M.; Kerminen, V.-M.; Anttila, T.; Laaksonen, A.; O'Dowd, C. D. Organic Aerosol Formation via Sulphate Cluster Activation. *Journal of Geophysical Research: Atmospheres* **2004**, *109* (D4), No. D04205.
(99) Kontkanen, J.; Stolzenburg, D.; Olenius, T.; Yan, C.; Dada, L.; Ahonen, L.; Simon, M.; Lehtipalo, K.; Riipinen, I. What Controls the Observed Size-Dependency of the Growth Rates of Sub-10 nm Atmospheric Particles? *Environ. Sci.: Atmos.* **2022**, *2* (3), 449−468.
(100) Schervish, M.; Donahue, N. M. Peroxy Radical Chemistry and the Volatility Basis Set. *Atmos Chem. Phys.* **2020**, *20* (2), 1183−1199.
(101) Semeniuk, K.; Dastoor, A. Current State of Aerosol Nucleation Parameterizations for Air-Quality and Climate Modeling. *Atmos. Environ.* **2018**, *179*, 77−106.
(102) Buenrostro Mazon, S.; Riipinen, I.; Schultz, D. M.; Valtanen, M.; Dal Maso, M.; Sogacheva, L.; Junninen, H.; Nieminen, T.; Kerminen, V.-M.; Kulmala, M. Classifying Previously Undefined Days from Eleven Years of Aerosol-Particle-Size Distribution Data from the SMEAR II Station, Hyytiälä, Finland. *Atmos Chem. Phys.* **2009**, *9* (2), 667−676.
(103) Yu, H.; Zhou, L.; Dai, L.; Shen, W.; Dai, W.; Zheng, J.; Ma, Y.; Chen, M. Nucleation and Growth of Sub-3nm Particles in the Polluted Urban atmosphere of a Megacity in China. *Atmos Chem. Phys.* **2016**, *16* (4), 2641−2657.
(104) Sebastian, M.; Kanawade, V. P.; Pierce, J. R. Observation of Sub-3 nm Particles and New Particle Formation at an Urban Location in India. *Atmos. Environ.* **2021**, *256*, No. 118460.
(105) Baalbaki, R.; Pikridas, M.; Jokinen, T.; Laurila, T.; Dada, L.; Bezantakos, S.; Ahonen, L.; Neitola, K.; Maisser, A.; Bimenyimana, E.; Christodoulou, A.; Unga, F.; Savvides, C.; Lehtipalo, K.; Kangasluoma, J.; Biskos, G.; Petäjä, T.; Kerminen, V.-M.; Sciare, J.; Kulmala, M. Towards Understanding the Characteristics of New Particle Formation in the Eastern Mediterranean. *Atmos Chem. Phys.* **2021**, *21* (11), 9223−9251.
(106) Dada, L.; Okuljar, M.; Shen, J.; Olin, M.; Wu, Y.; Heimsch, L.; Herlin, I.; Kankaanrinta, S.; Lampimäki, M.; Kalliokoski, J.; Baalbaki, R.; Lohila, A.; Petäjä, T.; Maso, M. D.; Duplissy, J.; Kerminen, V.-M.; Kulmala, M. The Synergistic Role of Sulfuric Acid, Ammonia and Organics in Particle Formation over an Agricultural Land. *Environ. Sci.: Atmos.* **2023**, *3* (8), 1195−1211.
(107) Link, M. F.; Robertson, R. L.; Shore, A.; Hamadani, B. H.; Cecelski, C. E.; Poppendieck, D. G. Ozone Generation and Chemistry from 222 nm Germicidal Ultraviolet Light in a Fragrant Restroom. *Environ. Sci.: Processes Impacts* **2024**, *26* (6), 1090−1106.
(108) Kulmala, M.; Junninen, H.; Dada, L.; Salma, I.; Weidinger, T.; Thén, W.; Vörösmarty, M.; Komsaare, K.; Stolzenburg, D.; Cai, R.; Yan,

https://doi.org/10.1021/acsestair.4c00118
ACS EST Air 2024, 1, 1276−1293

C.; Li, X.; Deng, C.; Jiang, J.; Petäjä, T.; Nieminen, T.; Kerminen, V.-M. Quiet New Particle Formation in the Atmosphere. *Front Environ. Sci.* **2022**, *10*, No. 912385.
(109) Lee, K.; Xue, J.; Geyh, A. S; Ozkaynak, H.; Leaderer, B. P; Weschler, C. J; Spengler, J. D Nitrous Acid, Nitrogen Dioxide, and Ozone Concentrations in Residential Environments. *Environ. Health Perspect.* **2002**, *110* (2), 145−150.
(110) Salonen, H.; Salthammer, T.; Morawska, L. Human Exposure to Ozone in School and Office Indoor Environments. *Environ. Int.* **2018**, *119*, 503−514.
(111) Morawska, L.; Tang, J. W.; Bahnfleth, W.; Bluyssen, P. M.; Boerstra, A.; Buonanno, G.; Cao, J.; Dancer, S.; Floto, A.; Franchimon, F.; Haworth, C.; Hogeling, J.; Isaxon, C.; Jimenez, J. L.; Kurnitski, J.; Li, Y.; Loomans, M.; Marks, G.; Marr, L. C.; Mazzarella, L.; Melikov, A. K.; Miller, S.; Milton, D. K.; Nazaroff, W.; Nielsen, P. V.; Noakes, C.; Peccia, J.; Querol, X.; Sekhar, C.; Seppänen, O.; Tanabe, S.; Tellier, R.; Tham, K. W.; Wargocki, P.; Wierzbicka, A.; Yao, M. How Can. Airborne Transmission of COVID-19 Indoors Be Minimised? *Environ. Int.* **2020**, *142*, No. 105832.
(112) Ma, L.; Zhang, Y.; Lin, Z.; Zhou, Y.; Yan, C.; Zhang, Y.; Zhou, W.; Ma, W.; Hua, C.; Li, X.; Deng, C.; Qi, Y.; Dada, L.; Li, H.; Bianchi, F.; Petäjä, T.; Kangasluoma, J.; Jiang, J.; Liu, S.; Hussein, T.; Kulmala, M.; Liu, Y. Deposition Potential of 0.003−10 μm Ambient Particles in the Humidified Human Respiratory Tract: Contribution of New Particle Formation Events in Beijing. *Ecotoxicol Environ. Saf* **2022**, *243*, No. 114023.
(113) Patra, S. S.; Wu, T.; Wagner, D. N.; Jiang, J.; Boor, B. E. Real-Time Measurements of Fluorescent Aerosol Particles in a Living Laboratory Office under Variable Human Occupancy and Ventilation Conditions. *Build Environ* **2021**, *205*, No. 108249.
(114) Kangasluoma, J.; Cai, R.; Jiang, J.; Deng, C.; Stolzenburg, D.; Ahonen, L. R.; Chan, T.; Fu, Y.; Kim, C.; Laurila, T. M.; Zhou, Y.; Dada, L.; Sulo, J.; Flagan, R. C.; Kulmala, M.; Petäjä, T.; Lehtipalo, K. Overview of Measurements and Current Instrumentation for 1−10 nm Aerosol Particle Number Size Distributions. *J. Aerosol Sci.* **2020**, *148*, No. 105584.
(115) Kangasluoma, J.; Junninen, H.; Lehtipalo, K.; Mikkilä, J.; Vanhanen, J.; Attoui, M.; Sipilä, M.; Worsnop, D.; Kulmala, M.; Petäjä, T. Remarks on Ion Generation for CPC Detection Efficiency Studies in Sub-3-nm Size Range. *Aerosol Sci. Technol.* **2013**, *47* (5), 556−563.
(116) Premnath, V.; Oberreit, D.; Hogan, C. J. Collision-Based Ionization: Bridging the Gap between Chemical Ionization and Aerosol Particle Diffusion Charging. *Aerosol. Sci. Technol.* **2011**, *45* (6), 712−726.
(117) Attoui, M.; Fernández-García, J.; Cuevas, J.; Vidal-de-Miguel, G.; Fernandez de la Mora, J. Charge Evaporation from Nanometer Polystyrene Aerosols. *J. Aerosol Sci.* **2013**, *55*, 149−156.
(118) Dada, L.; Stolzenburg, D.; Simon, M.; Fischer, L.; Heinritzi, M.; Wang, M.; Xiao, M.; Vogel, A. L.; Ahonen, L.; Amorim, A.; Baalbaki, R.; Baccarini, A.; Baltensperger, U.; Bianchi, F.; Daellenbach, K. R.; DeVivo, J.; Dias, A.; Dommen, J.; Duplissy, J.; Finkenzeller, H.; Hansel, A.; He, X.-C.; Hofbauer, V.; Hoyle, C. R.; Kangasluoma, J.; Kim, C.; Kürten, A.; Kvashnin, A.; Mauldin, R.; Makhmutov, V.; Marten, R.; Mentler, B.; Nie, W.; Petäjä, T.; Quéléver, L. L. J.; Saathoff, H.; Tauber, C.; Tome, A.; Molteni, U.; Volkamer, R.; Wagner, R.; Wagner, A. C.; Wimmer, D.; Winkler, P. M.; Yan, C.; Zha, Q.; Rissanen, M.; Gordon, H.; Curtius, J.; Worsnop, D. R.; Lehtipalo, K.; Donahue, N. M.; Kirkby, J.; El Haddad, I.; Kulmala, M. Role of Sesquiterpenes in Biogenic New Particle Formation. *Sci. Adv.* **2023**, *9* (36), No. eadi5297.
(119) Perez-Lorenzo, L. J.; Khanna, V.; Meena, T.; Schmitt, J. J.; de la Mora, J. F. A High Resolution DMA Covering the 1−67 nm Size Range. *Aerosol Sci. Technol.* **2020**, *54* (1), 128−142.
(120) Steiner, G.; Attoui, M.; Wimmer, D.; Reischl, G. P. A Medium Flow, High-Resolution Vienna DMA Running in Recirculating Mode. *Aerosol Sci. Technol.* **2010**, *44* (4), 308−315.
(121) Carslaw, N. Indoor Gas-Phase Chemistry. In *Handbook of Indoor Air Quality*; Springer Nature Singapore, 2022.
(122) Lew, M. M.; Dusanter, S.; Stevens, P. S. Measurement of Interferences Associated with the Detection of the hydroperoxy Radical in the Atmosphere Using Laser-Induced Fluorescence. *Atmos Meas Tech* **2018**, *11* (1), 95−109.
(123) Reichman, R.; Shirazi, E.; Colliver, D. G.; Pennell, K. G. US Residential Building Air Exchange Rates: New Perspectives to Improve Decision Making at Vapor Intrusion Sites. *Environ. Sci.: Processes Impacts* **2017**, *19* (2), 87−100.
(124) Patel, S.; Rim, D.; Sankhyan, S.; Novoselac, A.; Vance, M. E. Aerosol Dynamics Modeling of Sub-500 nm Particles during the HOMEChem Study. *Environ. Sci.: Processes Impacts* **2021**, *23* (11), 1706−1717.
(125) Wu, T.; Tasoglou, A.; Huber, H.; Stevens, P. S.; Boor, B. E. Influence of Mechanical Ventilation Systems and Human Occupancy on Time-Resolved Source Rates of Volatile Skin Oil Ozonolysis Products in a LEED-Certified Office Building. *Environ. Sci. Technol.* **2021**, *55* (24), 16477−16488.
(126) Li, M.; Weschler, C. J.; Bekö, G.; Wargocki, P.; Lucic, G.; Williams, J. Human Ammonia Emission Rates under Various Indoor Environmental Conditions. *Environ. Sci. Technol.* **2020**, *54* (9), 5419−5428.
(127) Mauldin III, R. L.; Berndt, T.; Sipilä, M.; Paasonen, P.; Petäjä, T.; Kim, S.; Kurtén, T.; Stratmann, F.; Kerminen, V.-M.; Kulmala, M. A New Atmospherically Relevant Oxidant of Sulphur Dioxide. *Nature* **2012**, *488* (7410), 193−196.
(128) Liao, K.-J.; Hou, X.; Baker, D. R. Impacts of Interstate Transport of Pollutants on High Ozone Events over the Mid-Atlantic United States. *Atmos. Environ.* **2014**, *84*, 100−112.
(129) Khamaganov, V. G.; Hites, R. A. Rate Constants for the Gas-Phase Reactions of Ozone with Isoprene, α- and β-Pinene, and Limonene as a Function of Temperature. *J. Phys. Chem. A* **2001**, *105* (5), 815−822.

https://doi.org/10.1021/acsestair.4c00118
ACS EST Air 2024, 1, 1276−1293